Title
Coupled charge and energy transfer dynamics in light harvesting complexes from a hybrid hierarchical equations of motion approach

Journal
The Journal of Chemical Physics, 157(17)

ISSN
0021-9606

Authors
Fay, Thomas P
Limmer, David T

Publication Date
2022-11-07

DOI
10.1063/5.0117659

Peer reviewed

RESEARCH ARTICLE | NOVEMBER 01 2022

Coupled charge and energy transfer dynamics in light harvesting complexes from a hybrid hierarchical equations of motion approach

Thomas P. Fay ; David T. Limmer

J. Chem. Phys. 157, 174104 (2022)
https://doi.org/10.1063/5.0117659
CHORUS

The Journal of Chemical Physics ARTICLE scitation.org/journal/jcp

Coupled charge and energy transfer dynamics in light harvesting complexes from a hybrid hierarchical equations of motion approach

Cite as: J. Chem. Phys. 157, 174104 (2022); doi: 10.1063/5.0117659
Submitted: 1 August 2022 • Accepted: 13 October 2022 •
Published Online: 1 November 2022

Thomas P. Fay[1,a] and David T. Limmer[1,2,3,4,b]

AFFILIATIONS

[1] Department of Chemistry, University of California, Berkeley, California 94720, USA
[2] Kavli Energy Nanoscience Institute at Berkeley, Berkeley, California 94720, USA
[3] Chemical Sciences Division, Lawrence Berkeley National Laboratory, Berkeley, California 94720, USA
[4] Materials Science Division, Lawrence Berkeley National Laboratory, Berkeley, California 94720, USA

[a] Author to whom correspondence should be addressed: tom.patrick.fay@gmail.com
[b] Electronic mail: dlimmer@berkeley.edu

ABSTRACT

We describe a method for simulating exciton dynamics in protein–pigment complexes, including effects from charge transfer as well as fluorescence. The method combines the hierarchical equations of motion, which are used to describe quantum dynamics of excitons, and the Nakajima–Zwanzig quantum master equation, which is used to describe slower charge transfer processes. We study the charge transfer quenching in light harvesting complex II, a protein postulated to control non-photochemical quenching in many plant species. Using our hybrid approach, we find good agreement between our calculation and experimental measurements of the excitation lifetime. Furthermore, our calculations reveal that the exciton energy funnel plays an important role in determining quenching efficiency, a conclusion we expect to extend to other proteins that perform protective excitation quenching. This also highlights the need for simulation methods that properly account for the interplay of exciton dynamics and charge transfer processes.

I. INTRODUCTION

Photosynthetic systems rely on both electronic excitation energy transfer (EET) and charge transfer (CT) processes to perform the reactions that sustain life on Earth.[1–5] For example, excitation energy transfer (EET) and charge transfer (CT) play fundamental roles in reaction centers,[4] where light energy from the Sun is harvested to drive chemical reactions. Charge transfer is also likely to have an important photo-protective function in photosynthetic organisms,[6–10] by quenching excess excitation energy and preventing damage to photosynthetic systems. The importance of coupled charge and excitation energy transfer dynamics necessitates the development of theoretical methods to accurately and efficiently simulate them together. Here, we develop a theory to study both processes using a hybrid approach that combines the hierarchical equation of motion (HEOM) with quantum master equations (QMEs) to afford a computationally efficient method that is also accurate.

Rapid excitation energy transfer has been studied extensively using a variety of methods, with HEOM emerging as a flexible and highly accurate approach for a large class of systems.[11–13] The HEOM method has enabled the simulation of EET in photosynthetic complexes without invoking perturbation theory, enabling a balanced description of both incoherent Förster EET and coherent excitonic EET as well as transport dynamics intermediate between these two regimes.[14] Although the HEOM method has been used extensively to study EET,[12,15–25] it has been used less in the study of combined EET and CT.[26] This is largely because charge transfer states typically couple much more strongly to the environment than local electronic excitations. Typical reorganization energies for CT processes are often in excess of $20k_BT$ at room temperature in polar environments due to the large changes in charge density distributions on molecules involved in CT[27] compared to $\sim 1k_BT$ for chlorophyll excitations. As a result of the large system–bath coupling strength, direct HEOM calculations involving CT states become very challenging.[28–30] Recent developments using

matrix product states,[31–33] and their generalizations,[34] or tree tensor networks[35] to solve the HEOM can help alleviate this problem, but these methods are limited to linear coupling models between the charge transfer states and harmonic environments. Alternative methods such as MACGIC-QUAPI[36,37] (a variant on the original QUAPI method[38–42]) have been successfully applied to models of coupled EET and CT in reaction centers,[37] but dynamics with this method can still be difficult to converge for large system sizes and strong system–bath coupling. Approximate theories, such as the modified-Redfield/generalized Förster theory,[43–45] have been applied to study CT processes in light harvesting complexes,[26,46,47] but these methods do not always accurately describe the EET dynamics in the absence of CT processes.[21] Semiclassical approaches have also been used to study exciton dynamics,[48–54] but these methods often break down for systems with large system–bath couplings as is encountered in CT processes. In order to facilitate the study of reaction center and CT quenching processes in photosynthesis, an accurate and computationally efficient method that can describe coupled EET and CT processes is needed.

In this work, we present a theory combining the HEOM method, which is used to model the EET dynamics of locally excited states, with quantum master equation approaches used to describe the charge transfer[55–58] and radiative processes.[19] Conceptually similar hybrid approaches in which different degrees of freedom are treated with different levels of theory have been used previously to extend the applicability of approximate theories,[59–62] but here we take the numerically exact HEOM method and make it more computationally tractable through judicious approximations on a subset of dynamical degrees of freedom. The working equations of our method, obtained using a Zwanzig projection approach,[63–65] are a set of simple linear differential equations for hierarchies of auxiliary density operators (ADOs) for the different manifolds of states in the system. Formally, the method can account for anharmonicity in the degrees of freedom coupled to the CT processes, though in this work, we only consider linear response models for the CT process. In Sec. II, we outline the model and the HEOM method, and in Sec. III, we derive the hybrid HEOM/QME method. In Sec. IV, we test the method against exact results for a dimer of locally excited states coupled to a CT state in order to verify the accuracy of the method. In Sec. V, we then apply the hybrid HEOM/QME method to study charge transfer quenching in light harvesting complex II (LHCII),[1,21,45,66,67] a system that would be intractable to study with direct HEOM calculations. Our simulations of LHCII reveal the importance of the excitation energy funnel in determining photo-protective quenching efficiency in the LHCII complex, a result that we discuss further in Sec. VI. Finally, we draw conclusions in Sec. VII.

II. THEORY

We consider the coupled energy and charge transfer of a photoexcited chromophore system, like that found in naturally occurring light harvesting complexes. In this section, we outline a general model Hamiltonian and review HEOM.

A. Exciton and charge transfer model

The system we consider consists of chromophores and electron donors and acceptors. An example of such a system is the

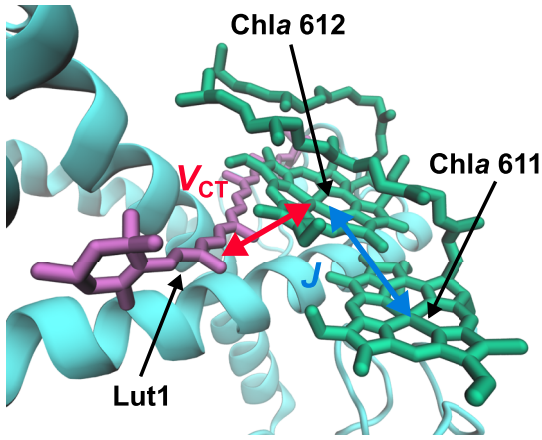

FIG. 1. tructure of the Chla611–Chla612 dimer in LHCII with the lutein (lutein 620 denoted Lut1 for brevity as in Ref. 67) electron donor (PDB 1RWT, chain C[68]). The electron transfer coupling is denoted by V_{CT} and the electrostatic inter-chromophore coupling is denoted by J.

Chl*a* 611–Chl*a* 612 dimer in LHCII shown in Fig. 1,[67] where the locally excited Chl*a* states couple to each other and the locally excited Chl*a* 612 can also accept an electron from the nearby lutein donor, which quenches the Chl*a** excitation. The chromophores have a ground state $|\mathrm{GS}\rangle$ and a manifold of singly excited states, which can be spanned by a local basis $|\mathrm{LE}_n\rangle$, which are coupled electrostatically. Such a system of coupled LE states can be well described by a Frenkel exciton model.[1] These locally excited states can also undergo charge transfer, where either the excited electron or hole transfers to a nearby acceptor or donor. For example, in the LHCII sub-system depicted in Fig. 1, the CT state is formed by electron transform from lutein to Chl*a* 612. The charge transfer states that can be formed by these processes are denoted as $|\mathrm{CT}_n\rangle$. These states can undergo charge recombination to return the system to $|\mathrm{GS}\rangle$. As well as coupling to each other, the LE and CT electronic excitations couple to the nuclear degrees of freedom on the chromophores, the donors/acceptors, and the surrounding polarizable environment, which leads to decoherence and relaxation of these excited electronic states. For example, if we consider the Chla dimer system depitced in Fig. 1,, the local excitation on each Chl*a* couples primarily to the vibrations localized on each chlorophyll,[1] but the CT excitation couples to the intramolecular Chl*a* and lutein vibrations, and the low frequency modes which determine polarization of the surrounding protein and solvent environment.[27] The different nature of the coupling to the environment for local and charge transfer excitations permits a partitioning of the environment into degrees of freedom that couple primarily to local excitations, the $\mathrm{b_{LE}}$ degrees of freedom, and the degrees of freedom that couple primarily to the charge transfer processes, denoted by $\mathrm{b_{CT}}$, a partitioning that will be explained in more detail below. Furthermore, the electronic states of the system couple to the electromagnetic (EM) field, which creates radiative decay pathways for the excited electronic states.[19]

The Hamiltonian for the system described above can be written as

$$\hat{H} = \hat{H}_{\mathrm{LE}} + \hat{H}_{\mathrm{CT}} + \hat{H}_{\mathrm{GS}} + \hat{H}_{\mathrm{LE,CT}} + \hat{H}_{\mathrm{CT,GS}} + \hat{H}_{\mathrm{EM}} + \hat{H}_{\mathrm{D}}, \quad (1)$$

where the ground-state Hamiltonian $\hat{H}_{\mathrm{GS}}$ decomposes as

$$\hat{H}_{\mathrm{GS}} = \hat{\Pi}_{\mathrm{GS}}(\hat{T} + \hat{V}_0). \tag{2}$$

Here, $\hat{T}$ is the nuclear kinetic energy operator, $\hat{V}_0$ is the ground-state potential energy operator, and $\hat{\Pi}_{\mathrm{GS}}$ is a projection operator $\hat{\Pi}_{\mathrm{GS}} = |\mathrm{GS}\rangle\langle\mathrm{GS}|$. Similarly, the Hamiltonian of the charge transfer states is

$$\hat{H}_{\mathrm{CT}} = \sum_{n=1}^{N_{\mathrm{CT}}} \hat{\Pi}_{\mathrm{CT}_n} \hat{H}_{\mathrm{CT}_n} = \sum_{n=1}^{N_{\mathrm{CT}}} \hat{\Pi}_{\mathrm{CT}_n}(\hat{T} + \hat{V}_{\mathrm{CT}_n}), \tag{3}$$

with $\hat{\Pi}_{\mathrm{CT}_n} = |\mathrm{CT}_n\rangle\langle\mathrm{CT}_n|$ being a projection operator onto the CT_n state, which we assume is a CT state in which electrons and holes are localized on specific acceptors and donors. For the locally excited states, we take a similar form but include all the LE state couplings J_{nm},

$$\hat{H}_{\mathrm{LE}} = \left(\sum_{n=1}^{N_{\mathrm{LE}}} |\mathrm{LE}_n\rangle\langle\mathrm{LE}_n|(E_n + \hat{T} + \hat{V}_{\mathrm{LE}_n}) + \sum_{n>m} J_{nm}(|\mathrm{LE}_n\rangle\langle\mathrm{LE}_m| + |\mathrm{LE}_m\rangle\langle\mathrm{LE}_n|)\right) \tag{4}$$

$$= \hat{H}_{\mathrm{LE,s}} + \sum_{n=1}^{N_{\mathrm{LE}}} |\mathrm{LE}_n\rangle\langle\mathrm{LE}_n|(\hat{T} + \hat{V}_{\mathrm{LE}_n}), \tag{5}$$

and we can again define an electronic projection operator $\hat{\Pi}_{\mathrm{LE}} = \sum_n |\mathrm{LE}_n\rangle\langle\mathrm{LE}_n|$, which commutes with $\hat{H}_{\mathrm{LE}}$. The CT-GS diabatic coupling term can be written as

$$\hat{H}_{\mathrm{CT,GS}} = \sum_{n=1}^{N_{\mathrm{CT}}} V_{\mathrm{CT}_n,\mathrm{GS}}(|\mathrm{CT}_n\rangle\langle\mathrm{GS}| + |\mathrm{GS}\rangle\langle\mathrm{CT}_n|) \tag{6}$$

and the locally excited state charge transfer diabatic coupling term can be written as

$$\hat{H}_{\mathrm{LE,CT}} = \sum_{n=1}^{N_{\mathrm{LE}}}\sum_{m=1}^{N_{\mathrm{CT}}} V_{\mathrm{LE}_n,\mathrm{CT}_m}(|\mathrm{LE}_n\rangle\langle\mathrm{CT}_m| + |\mathrm{CT}_m\rangle\langle\mathrm{LE}_n|), \tag{7}$$

with coupling constants $V_{\mathrm{CT}_n,\mathrm{GS}}$ and $V_{\mathrm{LE}_n,\mathrm{CT}_m}$. For simplicity, we have made the Condon approximation, by assuming that the diabatic state couplings have no nuclear coordinate dependence.

The electromagnetic field Hamiltonian $\hat{H}_{\mathrm{EM}}$ is given by[19,24]

$$\hat{H}_{\mathrm{EM}} = \sum_{\boldsymbol{k},p} \hbar\omega_{\boldsymbol{k}}\left(\hat{a}^{\dagger}_{\boldsymbol{k}p}\,\hat{a}_{\boldsymbol{k}p} + \frac{1}{2}\right), \tag{8}$$

where $\hat{a}_{\boldsymbol{k}p}$ is the electromagnetic (EM) field annihilation operator for mode $\boldsymbol{k}$ with polarization p and $\omega_{\boldsymbol{k}} = c_0|\boldsymbol{k}|$. These EM field modes are denoted by the b_{EM} degrees of freedom. $\hat{H}_{\mathrm{D}}$ is the dipole coupling operator between the molecular system and the EM field,[19,24,69]

$$\hat{H}_{\mathrm{D}} = -\hat{\boldsymbol{\mu}}\cdot\hat{\boldsymbol{\mathcal{E}}} \tag{9}$$

within a point dipole approximation for the system. Here, $\hat{\boldsymbol{\mu}}$ is the system transition dipole moment operator, with components for the LE_n state, $\hat{\mu}_{n,\alpha}$, with $\alpha = x, y, z$, given by

$$\hat{\mu}_{\alpha} = \sum_{n=1}^{N_{\mathrm{LE}}} \mu_{n,\alpha}(|\mathrm{LE}_n\rangle\langle\mathrm{GS}| + |\mathrm{GS}\rangle\langle\mathrm{LE}_n|), \tag{10}$$

and $\hat{\boldsymbol{\mathcal{E}}}$ is the electric field operator at the origin,

$$\hat{\boldsymbol{\mathcal{E}}} = i\sum_{\boldsymbol{k},p}\sqrt{\frac{\hbar\omega_{\boldsymbol{k}}}{2\mathcal{V}_0\,\varepsilon_0}}\left(\hat{a}_{\boldsymbol{k}p}\,\boldsymbol{e}_{\boldsymbol{k}p} - \hat{a}^{\dagger}_{\boldsymbol{k}p}\,\boldsymbol{e}^{*}_{\boldsymbol{k}p}\right), \tag{11}$$

where $\mathcal{V}_0$ is the volume of the system, ε_0 is the vacuum permittivity, and $\boldsymbol{e}_{\boldsymbol{k}p}$ is a unit vector defining the polarization of the EM field mode $\boldsymbol{k}p$.

In describing the potential energy surfaces for the different diabatic states, we start by separating out the nuclear bath coordinates that modulate the energy gap between the LE_n state and the ground state, which we denote the $\mathrm{b}_{\mathrm{LE}_n}$ degrees of freedom. This is justified by noting that the main degrees of freedom that modulate the LE_n energies are intramolecular vibrational modes on chromophore n and its surrounding local environment. Given the CT_n states involve these chromophores, the CT_n energies can also depend on the $\mathrm{b}_{\mathrm{LE}_n}$ degrees of freedom, as well as local modes on donors/acceptors involved in the charge transfer, and delocalized modes corresponding to environment polarization.[1,12] These additional bath degrees of freedom are denoted b_{CT}. In what follows, we assume that the b_{LE} and b_{CT} degrees of freedom are not coupled and are therefore uncorrelated, and the operators on these degrees of freedom, indicated by superscript b_{LE} and b_{CT} labels, therefore commute. This assumption is analogous to separating intramolecular and environmental contributions to spectral densities used in modeling condensed phase optical spectra[70–72] and the separation of inner- and outer-sphere contributions to electron transfer reorganization energies.[27,30]

Within this assumption, we can write down a model Hamiltonian for the coupled LE and CT states as

$$\hat{H} = \hat{H}_{\mathrm{LE,s}} + \sum_{n=1}^{N_{\mathrm{LE}}} |\mathrm{LE}_n\rangle\langle\mathrm{LE}_n|\Delta\hat{V}^{\mathrm{b}_{\mathrm{LE}_n}}_{\mathrm{LE}_n} + \sum_{n=1}^{N_{\mathrm{CT}}} \hat{\Pi}_{\mathrm{CT}_n}\left(\hat{H}_{\mathrm{CT}_n,\mathrm{s}} + \Delta\hat{V}^{\mathrm{b}_{\mathrm{CT}}}_{\mathrm{CT}_n} + \sum_{m=1}^{N_{\mathrm{LE}}} \Delta\hat{V}^{\mathrm{b}_{\mathrm{LE}_m}}_{\mathrm{CT}_n}\right) + \hat{H}^{\mathrm{b}_{\mathrm{LE}}}_{\mathrm{GS}} + \hat{H}^{\mathrm{b}_{\mathrm{CT}}}_{\mathrm{GS}} + \hat{H}_{\mathrm{ET}} + \hat{H}_{\mathrm{EM}} + \hat{H}_{\mathrm{D}}. \tag{12}$$

Here, $\hat{H}_{\mathrm{LE,s}}$ is the LE system Hamiltonian, containing the LE state energies and couplings, and similarly $\hat{H}_{\mathrm{CT}_n,\mathrm{s}}$ is the system Hamiltonian for CT_n, which describes the energy of CT_n and $\hat{H}_{\mathrm{ET}} = \hat{H}_{\mathrm{LE,CT}} + \hat{H}_{\mathrm{CT,GS}}$. $\Delta\hat{V}^{\mathrm{b}_{\mathrm{LE}_n}}_{\mathrm{LE}_n} = \hat{V}_{\mathrm{LE}_n} - \hat{V}_0$ describes how the potential energy surface of the ground state is perturbed by the electronic excitation LE_n; similarly, $\Delta\hat{V}^{\mathrm{b}_{\mathrm{CT}}}_{\mathrm{CT}_n} + \sum_m \Delta\hat{V}^{\mathrm{b}_{\mathrm{LE}_m}}_{\mathrm{CT}_n} = \hat{V}_{\mathrm{CT}_n} - \hat{V}_0$ describes how the ground state potential is shifted in the charge transfer state CT_n. The potential energy shift for the CT states is divided into a sum of terms that are correlated with the LE_m energy shifts, $\Delta\hat{V}^{\mathrm{b}_{\mathrm{LE}_m}}_{\mathrm{CT}_n}$, corresponding to reorganization of the intramolecular modes on each chromophore, and the remaining uncorrelated component $\Delta\hat{V}^{\mathrm{b}_{\mathrm{CT}}}_{\mathrm{CT}_n}$. The reference ground state potentials for the b_{LE} and b_{CT} degrees of freedom are given by $\hat{H}^{\mathrm{b}_{\mathrm{LE}}}_{\mathrm{GS}}$ and $\hat{H}^{\mathrm{b}_{\mathrm{CT}}}_{\mathrm{GS}}$, respectively.

B. The LE state potential energy surfaces

We can often assume that the LE state energy shift operators $\Delta\hat{V}^{\mathrm{b_{LE}}_n}_{\mathrm{LE}_n}$ have Gaussian statistics in the ground state reference ensemble, meaning the third- and higher-order cumulants vanish. Furthermore, we assume that the correlation functions of $\Delta\hat{V}^{\mathrm{b_{LE}}_n}_{\mathrm{LE}_n}$ can be decomposed into a sum of contributions as follows:[12,14]

$$\left\langle \Delta V^{\mathrm{b_{LE}}_n}_{\mathrm{LE}_n}(t)\Delta\hat{V}^{\mathrm{b_{LE}}_m}_{\mathrm{LE}_m}(0)\right\rangle_{\mathrm{b_{LE}}} = \delta_{n,m}\sum_{r=1}^{N_{\mathrm{b},n}} C_{n,r}(t), \tag{13}$$

where $\langle\cdots\rangle_{\mathrm{b_{LE}}} = \mathrm{Tr}_{\mathrm{b_{LE}}}[\cdots e^{-\beta\hat{H}^{\mathrm{b_{LE}}}_{\mathrm{GS}}}]/\mathrm{Tr}_{\mathrm{b_{LE}}}[e^{-\beta\hat{H}^{\mathrm{b_{LE}}}_{\mathrm{GS}}}]$ and $\Delta V^{\mathrm{b_{LE}}_n}_{\mathrm{LE}_n}(t) = e^{i\hat{H}^{\mathrm{b_{LE}}}_{\mathrm{GS}}t/\hbar}\Delta V^{\mathrm{b_{LE}}_n}_{\mathrm{LE}_n}e^{-i\hat{H}^{\mathrm{b_{LE}}}_{\mathrm{GS}}t/\hbar}$. Provided $C^{\mathrm{b_{LE}}}_{n,r}(t)$ is a smooth function, it can be written in terms of a spectral density $\mathcal{J}_{n,r}(\omega)$ as

$$C^{\mathrm{b_{LE}}}_{n,r}(t) = \frac{\hbar}{\pi}\int_0^\infty \mathrm{d}\omega\,\mathcal{J}_{n,r}(\omega)\left[\coth\left(\frac{\beta\hbar\omega}{2}\right)\cos(\omega t) - i\,\sin(\omega t)\right]. \tag{14}$$

With these assumptions, $\hat{H}^{\mathrm{b_{LE}}}_{\mathrm{GS}}$ can be written as a sum of independent harmonic bath Hamiltonians and the LE state energy shift terms $\Delta\hat{V}^{\mathrm{b_{LE}}_n}_{\mathrm{LE}_n}$ are linear in the bath mode displacements.[13] These assumptions are widely used in describing exciton dynamics and largely hold due to the relatively weak coupling between the LE states and the environment, meaning shifts in the potential energy surfaces can be well approximated as simple shifts in a harmonic potential.[1,12] Overall, this means that we can write the $\mathrm{b_{LE}}$ Hamiltonians as[12]

$$\hat{H}^{\mathrm{b_{LE}}}_{\mathrm{GS}} = \sum_{n=1}^{N_{\mathrm{LE}}}\sum_{r=1}^{N_{\mathrm{b},n}}\sum_{\alpha=1}^{N_{n,r}}\left(\frac{\hat{p}^2_{nr\alpha}}{2m_{nr\alpha}} + \frac{1}{2}m_{nr\alpha}\omega^2_{nr\alpha}\hat{q}^2_{nr\alpha}\right), \tag{15}$$

$$\Delta\hat{V}^{\mathrm{b_{LE}}_n}_{\mathrm{LE}_n} = \sum_{r=1}^{N_{\mathrm{b},n}}\hat{B}_{n,r} = \sum_{r=1}^{N_{\mathrm{b},n}}\sum_{\alpha=1}^{N_{n,r}} c_{nr\alpha}\,\hat{q}_{nr\alpha}, \tag{16}$$

where the bath mode frequencies $\omega_{nr\alpha}$ and coupling coefficients $c_{nr\alpha}$ of the mode displacement operators $\hat{q}_{nr\alpha}$ appear in the bath coupling operators $\hat{B}_{nr\alpha}$. We also assume that the $\Delta\hat{V}^{\mathrm{b_{LE}}_m}_{\mathrm{CT}_n}$ terms, which describe the correlation between the CT state and the LE state energy shifts, can be written as linear in the $\mathrm{b_{LE}}$ bath coupling operators in Eq. (16), with coupling coefficients $\kappa^{\mathrm{CT}_n}_{m,r}$,

$$\Delta\hat{V}^{\mathrm{b_{LE}}_m}_{\mathrm{CT}_n} = \sum_{r=1}^{N_{m,r}}\kappa^{\mathrm{CT}_n}_{m,r}\,\hat{B}_{m,r}. \tag{17}$$

We can evaluate the spectral density for each bath, i.e.,

$$\mathcal{J}_{n,r}(\omega) = \frac{\pi}{2}\sum_{\alpha=1}^{N_{n,r}}\frac{c^2_{nr\alpha}}{m_{nr\alpha}\,\omega_{nr\alpha}}\delta(\omega-\omega_{nr\alpha}) \tag{18}$$

in terms of these microscopic parameters in the Hamiltonian.

C. The hierarchical equations of motion

The hierarchical equations of motion provide a method for simulating the dynamics of a system linearly coupled to a harmonic bath. It was developed for Hamiltonians, like the ones we are interested in, that can be decomposed as[13]

$$\hat{H} = \hat{H}_{\mathrm{s}} + \sum_{j=1}^{N_{\mathrm{b}}}\left(\hat{H}_{\mathrm{b},j} + \hat{V}_j\hat{B}_j\right), \tag{19}$$

where $\hat{H}_{\mathrm{s}}$ is the sub-system Hamiltonian, $\hat{V}_j$ are system operators, and $\hat{H}_{\mathrm{b},j}$ is the Hamiltonian of harmonic bath j. The bath displacement operators, $\hat{B}_j$, are defined as $\hat{H}_{\mathrm{b},j} = \sum_{\alpha=1}^{N_j}\hat{p}^2_{j\alpha}/2m_{j\alpha} + m_{j\alpha}\omega^2_{j\alpha}\hat{q}^2_{j\alpha}/2$ and $\hat{B}_j = \sum_{\alpha=1}^{N_j} c_{j,\alpha}\,\hat{q}_{j,\alpha}$. as analogous to Eqs. (15) and (16), where the index n,r is replaced with a single index j. Assuming the bath displacement operator correlation functions can be decomposed as

$$C_j(t) = \sum_{k=1}^{\infty} a_{jk}e^{-\nu_{jk}t} \tag{20}$$

and using the Gaussian property of the harmonic baths, we can obtain the system reduced density operator $\hat{\rho}(t) = \mathrm{Tr}_{\mathrm{b}}[\hat{\rho}_{\mathrm{tot}}(t)]$, from a hierarchy of auxiliary density operators (ADOs) $\hat{\rho}_{\mathbf{n}}(t)$ obeying the following equation of motion:[11,13,73]

$$\begin{aligned}\frac{\mathrm{d}}{\mathrm{d}t}\hat{\rho}_{\mathbf{n}}(t) = &-\frac{i}{\hbar}\left[\hat{H}_{\mathrm{s}},\hat{\rho}_{\mathbf{n}}(t)\right] - \sum_{j,k} n_{jk}\,\nu_{jk}\,\hat{\rho}_{\mathbf{n}}(t) + \Xi_{\mathbf{n}}\,\hat{\rho}_{\mathbf{n}}(t)\\ &- \frac{i}{\hbar}\sum_{j,k}\sqrt{(n_{jk}+1)|a_{jk}|}\left[\hat{V}_j,\hat{\rho}_{\mathbf{n}^+_{jk}}\right]\\ &- \frac{i}{\hbar}\sum_{j,k}\sqrt{\frac{n_{jk}}{|a_{jk}|}}\left(a_{jk}\,\hat{V}_j\,\hat{\rho}_{\mathbf{n}^-_{jk}} - a^*_{jk}\,\hat{\rho}_{\mathbf{n}^-_{jk}}\,\hat{V}_j\right),\end{aligned} \tag{21}$$

where $\mathbf{n} = (n_{1,0}, n_{1,1}, \ldots, n_{j,k}, \ldots)$ is a multi-index that specifies the excitation level of mode k for each bath j for a given hierarchy element, $\mathbf{n}^{\pm}_{jk} = (n_{1,0}, n_{1,1}, \ldots, n_{j,k} \pm 1, \ldots)$, and $\Xi_{\mathbf{n}}$ is a system superoperator that accounts for finite truncation of the hierarchy. The sub-system reduced density operator can be obtained as the zeroth element of this hierarchy, $\hat{\rho}(t) = \hat{\rho}_{\mathbf{0}}(t)$.

We can write down the truncated hierarchy as

$$|\rho(t)\rangle\rangle = \sum_{\mathbf{n}}|\rho_{\mathbf{n}}(t)\rangle\rangle\otimes|\mathbf{n}\rangle\rangle, \tag{22}$$

where $|\mathbf{n}\rangle\rangle$ is a basis vector corresponding to the auxiliary density operator $\mathbf{n}$ and $|\rho_{\mathbf{n}}(t)\rangle\rangle$ is the Liouville space vector of this ADO. With this notation, we can write down the equation of motion more compactly as[29,33,74]

$$\frac{\mathrm{d}}{\mathrm{d}t}|\rho(t)\rangle\rangle = \mathcal{L}|\rho(t)\rangle\rangle \tag{23}$$

$$= (\mathcal{L}_{\mathrm{s}}\otimes\mathcal{I}_{\mathrm{ado}} - \mathcal{I}_{\mathrm{s}}\otimes\Gamma + \Xi + \mathcal{V})|\rho(t)\rangle\rangle, \tag{24}$$

where $\mathcal{L}_{\mathrm{s}} = -(i/\hbar)[\hat{H}_{\mathrm{s}},\ \cdot\ ]$ is the system Liouvillian, $\mathcal{I}_{\mathrm{s}}$ and $\mathcal{I}_{\mathrm{ado}}$ are identity operators on the system Liouville space and the set of ADOs respectively, $\Gamma = \sum_{\mathbf{n}}\gamma_{\mathbf{n}}|\mathbf{n}\rangle\rangle\langle\langle\mathbf{n}|$ is a matrix of ADO decay rates, $\Xi = \sum_{\mathbf{n}\in\mathcal{N}}\Xi_{\mathbf{n}}\otimes|\mathbf{n}\rangle\rangle\langle\langle\mathbf{n}|$ is a superoperator that accounts for finite truncation of the hierarchy,[73] and $\mathcal{V}$ is the term that couples different ADOs within the hierarchy. Henceforth, we will swap between the Liouville vector notation $|\rho\rangle\rangle$ and standard operator notation $\hat{\rho}$, as is most appropriate.

III. THE HYBRID HEOM/QME METHOD

Using HEOM to study CT in these systems can be difficult due to the large reorganization energies involved, which give rise to large values of a_{jk} for baths associated with CT processes. The large coupling coefficients for certain modes means many ADOs are needed to converge the HEOM dynamics. This can make HEOM calculations involving CT states intractable when there are large numbers of system states and baths. A simplification results as the reorganization energy of the charge transfer processes is typically much larger than the electronic coupling between CT states and LE states, and thus the use of perturbation theory, where the coupling to the CT states is treated as a small parameter, can be expected to give an accurate description of the coupled dynamics of the LE and CT states.[27,56,57] In this section, we describe how Zwanzig projection can be used to construct a hybrid HEOM/QME method in which radiative and electron transfer processes are treated with perturbation theory while preserving the high accuracy of the EET dynamics afforded by HEOM. Similar approaches have been used to derive hybrid HEOM methods to describe radiative processes in EET in protein–pigment complexes,[19,23,75] but these have not included charge transfer processes. The approach taken here combines some of the ideas for describing radiative processes in Ref. 19 with the Nakajima–Zwanzig theory-based approaches that have been used to derive quantum master equations for spin density operators of different charge transfer states in photoexcited molecules.[56–58]

A. Zwanzig projection

Here, we use the Zwanzig projection operator approach to construct a hybrid HEOM/QME method. We set up the problem by formally including the $\mathrm{b_{CT}}$ and EM field degrees of freedom as well as the full set of electronic states, in the system Hamiltonian $\hat{H}_\mathrm{s}$ in the hierarchical equations of motion. This means that the "system" Hamiltonian is taken to be

$$\hat{H}_\mathrm{s} = \hat{H}_\mathrm{LE,s} + \sum_{n=1}^{N_\mathrm{CT}} \hat{\Pi}_{\mathrm{CT}_n}\left(\hat{H}_{\mathrm{CT}_n,\mathrm{s}} + \Delta\hat{V}^{\mathrm{b_{CT}}}_{\mathrm{CT}_n}\right) + \hat{H}^{\mathrm{b_{CT}}}_\mathrm{GS} + \hat{H}_\mathrm{LE,CT} + \hat{H}_\mathrm{CT,GS} + \hat{H}_\mathrm{EM} + \hat{H}_\mathrm{D}. \tag{25}$$

The response of the system to the $\mathrm{b_{LE}}$ couplings is treated with the HEOM, with the set of $N_{\mathrm{b_{LE}}} = \sum_n N_{\mathrm{b},n}$ LE baths indexed by $j = n, r$, and

$$\hat{V}_{n,r} = |\mathrm{LE}_n\rangle\langle\mathrm{LE}_n| + \sum_{m=1}^{N_\mathrm{CT}} \kappa^{\mathrm{CT}_m}_{n,r}\,\hat{\Pi}_{\mathrm{CT}_m}, \tag{26}$$

are the set of system–bath coupling operators. The coefficients $\kappa^{\mathrm{CT}_m}_{n,r}$ here describe how the $\mathrm{b_{LE}}$ degrees of freedom are coupled to the CT states as defined in Eq. (17).

The main variables of interest for this system, when the $\mathrm{b_{LE}}$ degrees of freedom are treated with the HEOM method, are the reduced density operators for the LE states and the CT and GS state populations. These populations are given by

$$\hat{\sigma}_{A,\mathrm{s}}(t) = \hat{\Pi}_A\,\mathrm{Tr}_{\mathrm{b}'}[\hat{\rho}_\mathbf{0}(t)]\hat{\Pi}_A, \tag{27}$$

where $\hat{\rho}_\mathbf{0}(t)$ is the zeroth ADO of the hierarchy, $\hat{\Pi}_A$ is a projection operator onto the manifold of electronic states with $A = \mathrm{LE}$, CT_n or GS, and $\mathrm{Tr}_{\mathrm{b}'}$ denotes a trace over all $\mathrm{b_{CT}}$ and $\mathrm{b_{EM}}$ field degrees of freedom, which we collectively refer to as b'. Since we aim to treat the exciton dynamics with the HEOM, we construct the projection operator for the HEOM ADOs as

$$\mathcal{P} = \sum_A \mathcal{P}_A \otimes \mathcal{I}_\mathrm{ado}, \tag{28}$$

$$\mathcal{P}_A = \hat{\rho}^{\mathrm{b_{CT}}}_A \hat{\rho}^{\mathrm{b_{EM}}}\hat{\Pi}_A\,\mathrm{Tr}_{\mathrm{b}'}[\,\cdot\,]\hat{\Pi}_A. \tag{29}$$

Here, the local equilibrium density operator for the $\mathrm{b_{CT}}$ degrees of freedom in state A is $\hat{\rho}^{\mathrm{b_{CT}}}_A = e^{-\beta\hat{H}^{\mathrm{b_{CT}}}_A}/\mathrm{Tr}_{\mathrm{b_{CT}}}[e^{-\beta\hat{H}^{\mathrm{b_{CT}}}_A}]$, and $\hat{H}^{\mathrm{b_{CT}}}_A = \hat{H}^{\mathrm{b_{CT}}}_\mathrm{GS}$ for $A = \mathrm{GS}$ or LE, where

$$\hat{H}^{\mathrm{b_{CT}}}_{\mathrm{CT}_n} = \hat{H}^{\mathrm{b_{CT}}}_\mathrm{GS} + \Delta\hat{V}^{\mathrm{b_{CT}}}_{\mathrm{CT}_n}, \tag{30}$$

with the terms here defined as in Eq. (12). The EM field density operator is approximated as the zero temperature equilibrium density operator of the bare EM field, where all field modes are in their ground state, $\hat{\rho}^{\mathrm{b_{EM}}} = \otimes_{\boldsymbol{k},p}|0_{\boldsymbol{k}p}\rangle\langle 0_{\boldsymbol{k}p}|$. This approximation is justified by the fact that we are only interested in spontaneous emission processes since the field modes at the LE state energies are not thermally excited at ambient temperatures, therefore, $\beta\hbar\omega_{\boldsymbol{k}p} \approx 0$ for field modes resonant with the LE-GS energy gaps. This type of projection operator is analogous to that used in Refs. 56 and 57 for electronic state spin density operators. This projected density operator contains the reduced density operator hierarchy, $|\sigma_A(t)\rangle\rangle$, for each electronic state A,

$$\mathcal{P}|\rho(t)\rangle\rangle = \sum_A |\rho^{\mathrm{b_{CT}}}_A\rangle\rangle \otimes |\rho^{\mathrm{b_{EM}}}\rangle\rangle \otimes |\sigma_A(t)\rangle\rangle, \tag{31}$$

$$|\sigma_A(t)\rangle\rangle = \sum_\mathbf{n} |\sigma_{A,\mathbf{n}}(t)\rangle\rangle \otimes |\mathbf{n}\rangle\rangle, \tag{32}$$

$$\hat{\sigma}_{A,\mathbf{n}}(t) = \hat{\Pi}_A\,\mathrm{Tr}_{\mathrm{b}'}[\hat{\rho}_\mathbf{n}(t)]\hat{\Pi}_A. \tag{33}$$

An example of the partitioning into separate hierarchies for different state manifolds, $|\sigma_A(t)\rangle\rangle$, is illustrated in Fig. 2 for a system with four LE states, two CT states, and the ground state.

Using this projection operator $\mathcal{P}$, we can obtain a quantum master equation for the projected hierarchy of ADOs $\mathcal{P}|\rho(t)\rangle\rangle$ using the Nakajima–Zwanzig equation,[63–65]

$$\frac{\mathrm{d}}{\mathrm{d}t}\mathcal{P}|\rho(t)\rangle\rangle = \mathcal{P}\mathcal{L}\mathcal{P}|\rho(t)\rangle\rangle + \int_0^t \mathcal{K}(t-\tau)\mathcal{P}|\rho(\tau)\rangle\rangle\,\mathrm{d}\tau, \tag{34}$$

where the memory kernel $\mathcal{K}(t)$ is given by

$$\mathcal{K}(t) = \mathcal{P}\mathcal{L}e^{(1-\mathcal{P})\mathcal{L}t}(1-\mathcal{P})\mathcal{L}\mathcal{P}. \tag{35}$$

The generalized master equations for $|\sigma_A(t)\rangle\rangle$ can be straightforwardly obtained from this by tracing out the $\mathrm{b_{CT}}$ and $\mathrm{b_{EM}}$ degrees

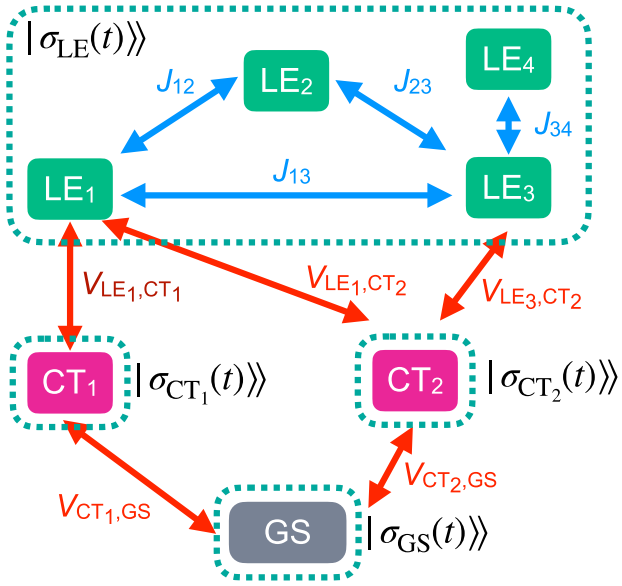

FIG. 2. chematic of the states, interstate coupling, and partitioning into reduced hierarchies $|\sigma_A(t)\rangle\rangle$ for an example system with four LE states, two CT states, and the GS.

of freedom. This gives the following general hybrid HEOM/QME for $|\sigma_A(t)\rangle\rangle$:

$$\frac{\mathrm{d}}{\mathrm{d}t}|\sigma_A(t)\rangle\rangle = \mathcal{L}_A|\sigma_A(t)\rangle\rangle + \sum_B \int_0^t \mathcal{K}_{AB}(t-\tau)|\sigma_B(\tau)\rangle\rangle \mathrm{d}\tau, \tag{36}$$

where $\mathcal{L}_A = \langle\langle 1_{b'}|\mathcal{P}_A\mathcal{L}\mathcal{P}_A|\rho_A^{b'}\rangle\rangle$ is the component of $\mathcal{P}\mathcal{L}\mathcal{P}$ that acts on $|\sigma_A(t)\rangle\rangle$ and similarly $\mathcal{K}_{AB}(t)$ is the component of $\mathcal{K}_{AB}(t) = \langle\langle 1_{b'}|\mathcal{P}_A\mathcal{K}(t)\mathcal{P}_B|\rho_B^{b'}\rangle\rangle$ that couples $|\sigma_B(t)\rangle\rangle$ to $|\sigma_A(t)\rangle\rangle$. Here, $|1_{b'}\rangle\rangle$ is the identity operator on the b_{CT} and EM degrees of freedom and $|\rho_A^{b'}\rangle\rangle = |\rho_A^{b_{CT}}\rangle\rangle \otimes |\rho^{b_{EM}}\rangle\rangle$ and the Liouville space inner product is $\langle\langle A|B\rangle\rangle = \mathrm{Tr}[\hat{A}^\dagger\hat{B}]$.

B. Approximating the exact master equation

While Eq. (36) is formally exact, evaluating the kernel requires evaluation of the exact dynamics generated by $\mathcal{L}$, which is difficult due to the large Hilbert space associated with b_{CT} and b_{EM}. However, in the absence of the excitonic dynamics, each can be treated accurately with simplifying approximations. First, we make the Markovian approximation, in which we assume the decay time scale of $\mathcal{K}_{AB}(t)$ is much faster than the dynamics of $|\sigma_A(t)\rangle\rangle$, and therefore we approximate the time-convolution terms as[55,56]

$$\int_0^t \mathcal{K}_{AB}(t-\tau)|\sigma_B(\tau)\rangle\rangle\, \mathrm{d}\tau \approx \int_0^\infty \mathcal{K}_{AB}(\tau)\, \mathrm{d}\tau |\sigma_B(t)\rangle\rangle. \tag{37}$$

Second, we approximate the full kernel in Eq. (35) with its second order approximation in perturbation theory.[55,56] Here, the perturbation Liouvillian $\mathcal{L}_V$ is taken to be

$$\mathcal{L}_V = \mathcal{L}_{ET} + \mathcal{L}_R, \tag{38}$$

$$\mathcal{L}_{ET} = -\frac{i}{\hbar}[\hat{H}_{ET}, \cdot\,] \otimes \mathcal{I}_{ado}, \tag{39}$$

$$\mathcal{L}_R = -\frac{i}{\hbar}[\hat{H}_D, \cdot\,] \otimes \mathcal{I}_{ado}, \tag{40}$$

where $\hat{H}_{ET}$ is given by Eq. (12) and $\hat{H}_D$ is given by Eq. (9). With this, the kernel $\mathcal{K}(t)$ can be approximated as

$$\mathcal{K}(t) \approx \mathcal{K}^{(2)}(t) = \mathcal{P}\mathcal{L}_V e^{(\mathcal{L}_0+\mathcal{V})t}\mathcal{L}_V\mathcal{P}, \tag{41}$$

where we have defined

$$\mathcal{L}_0 = \mathcal{L} - \mathcal{L}_V - \mathcal{V}. \tag{42}$$

Because the baths are uncorrelated, the second order kernel can be split as

$$\mathcal{K}^{(2)}(t) = \mathcal{K}^{(2)}_{ET}(t) + \mathcal{K}^{(2)}_R(t) \tag{43}$$

$$= \mathcal{P}\mathcal{L}_{ET}e^{(\mathcal{L}_0+\mathcal{V})t}\mathcal{L}_{ET}\mathcal{P} + \mathcal{P}\mathcal{L}_R e^{(\mathcal{L}_0+\mathcal{V})t}\mathcal{L}_R\mathcal{P}, \tag{44}$$

into an electron transfer term, $\mathcal{K}^{(2)}_{ET}(t)$, and a radiative decay term, $\mathcal{K}^{(2)}_R(t)$.

The final simplification we make is to approximate the reference propagator $e^{(\mathcal{L}_0+\mathcal{V})t}$ appearing in the ET kernel as

$$e^{(\mathcal{L}_0+\mathcal{V})t} \approx e^{(\mathcal{L}_0+\tilde{\mathcal{V}})t}, \tag{45}$$

where $\tilde{\mathcal{V}} = \sum_{\mathbf{n},\mathbf{n}'\in\mathcal{N}_K}|\mathbf{n}\rangle\rangle\langle\langle\mathbf{n}|\mathcal{V}|\mathbf{n}'\rangle\rangle\langle\langle\mathbf{n}'|$ is $\mathcal{V}$ projected onto a subset of the ADOs. We make this approximation to reduce the density of the coupling between elements of $|\sigma_A(t)\rangle\rangle$ in the equations of motion and increase the computational efficiency of the method. For the radiative decay term, we simply approximate $e^{(\mathcal{L}_0+\mathcal{V})t} \approx e^{\mathcal{L}_{0,s}t}$, where $\mathcal{L}_{0,s}$ is just the coherent system dynamics term appearing in $\mathcal{L}_0$. In deriving explicit expressions for terms appearing in the hybrid HEOM/QME, it is important to note that $\mathcal{L}_0$ and $\mathcal{V}$ can be decomposed as $\mathcal{L}_0 = \oplus_{A,B}\mathcal{L}_0^{AB}$ and $\mathcal{V} = \oplus_{A,B}\mathcal{V}^{AB}$, where each term only acts on coherences $|A\rangle\langle B|$ between electronic states in manifolds A and B.

Applying the above set of approximations to Eq. (36) allows us to write the hybrid HEOM/QME as

$$\frac{\mathrm{d}}{\mathrm{d}t}|\sigma_A(t)\rangle\rangle = \mathcal{L}_A|\sigma_A(t)\rangle\rangle + \sum_B \mathcal{R}_{AB}|\sigma_B(t)\rangle\rangle, \tag{46}$$

where $\mathcal{R}_{AB}$ can be written as a sum of electron transfer and radiative decay terms, $\mathcal{R}_{AB} = \mathcal{R}^{ET}_{AB} + \mathcal{R}^{R}_{AB}$. We can write this system of equations more explicitly as

$$\begin{aligned}\frac{\mathrm{d}}{\mathrm{d}t}\hat{\sigma}_{A,\mathbf{n}}(t) = &-\frac{i}{\hbar}[\hat{H}_{A,s}, \hat{\sigma}_{A,\mathbf{n}}(t)] - \gamma_{\mathbf{n}}\,\hat{\sigma}_{A,\mathbf{n}}(t) \\ &+ \Xi_{A,\mathbf{n}}\,\hat{\sigma}_{A,\mathbf{n}}(t) - \frac{i}{\hbar}\sum_{j,k}\sqrt{(n_{jk}+1)|a_{jk}|}[\hat{V}_{A,j}, \hat{\sigma}_{A,\mathbf{n}^+_{jk}}(t)] \\ &- \frac{i}{\hbar}\sum_{j,k}\sqrt{\frac{n_{jk}}{|a_{jk}|}}\left(a_{jk}\,\hat{V}_{A,j}\,\hat{\sigma}_{A,\mathbf{n}^-_{jk}}(t) - a^*_{jk}\,\hat{\sigma}_{A,\mathbf{n}^-_{jk}}(t)\hat{V}_{A,j}\right) \\ &+ \sum_B\sum_{\mathbf{n}'}\mathcal{R}_{AB,\mathbf{n}\mathbf{n}'}\,\hat{\sigma}_{B,\mathbf{n}'}(t),\end{aligned} \tag{47}$$

where $\hat{H}_{A,s}$ and $\hat{V}_{A,j}$ are the components of the electronic state terms in $\hat{H}_s$ and $\hat{V}_j$ projected onto the manifold of electronic states A (i.e., $\hat{V}_{A,j} = \hat{\Pi}_A \hat{V}_j \hat{\Pi}_A$), $\Xi_{A,\mathbf{n}}$ is a superoperator that accounts for finite truncation, projected on A, and $\mathcal{R}_{AB,\mathbf{nn}'}$ is the component of $\mathcal{R}_{AB}$ that couples state $\hat{\sigma}_{A,\mathbf{n}}(t)$ to $\hat{\sigma}_{B,\mathbf{n}'}(t)$. Now that we have the general form of the Markovian hybrid HEOM/QME, we just need to evaluate the transfer operators $\mathcal{R}^{\mathrm{ET}}_{AB}$ and $\mathcal{R}^{\mathrm{R}}_{AB}$. This is detailed in the following sections.

C. The electron transfer term

We start by considering the electron transfer term, $\mathcal{R}^{\mathrm{ET}}_{AB}$. By noting that $\mathcal{L}_0 + \tilde{\mathcal{V}}$ does not mix populations and coherences between the LE, CT, and GS manifolds, the elements of $\mathcal{R}^{\mathrm{ET}}_{AB}$ where $A \neq B$ can be evaluated straightforwardly as

$$\mathcal{R}^{\mathrm{ET}}_{AB} = \mathcal{L}^{\mathrm{L},AB}_{H_{\mathrm{ET}}} \mathcal{G}^{B}_{AB} \mathcal{L}^{\mathrm{R},BA}_{H_{\mathrm{ET}}} + \mathcal{L}^{\mathrm{R},BA}_{H_{\mathrm{ET}}} \mathcal{G}^{B}_{BA} \mathcal{L}^{\mathrm{L},AB}_{H_{\mathrm{ET}}}, \tag{48}$$

where the $\mathcal{L}^{\mathrm{L/R},AB}_{H_{\mathrm{ET}}}$ terms are given by

$$\mathcal{L}^{\mathrm{L},AB}_{H_{\mathrm{ET}}} \hat{\sigma} = \frac{1}{\hbar} \hat{\Pi}_A \hat{H}_{\mathrm{ET}} \hat{\Pi}_B \hat{\sigma} \tag{49}$$

$$\mathcal{L}^{\mathrm{R},BA}_{H_{\mathrm{ET}}} \hat{\sigma} = \frac{1}{\hbar} \hat{\sigma} \hat{\Pi}_B \hat{H}_{\mathrm{ET}} \hat{\Pi}_A \tag{50}$$

and the $\mathcal{G}^{C}_{AB}$ terms are given by

$$\mathcal{G}^{B}_{AB} = \int_0^\infty \mathrm{d}t\, G^{B}_{AB}(t) \mathcal{S}^{\mathrm{ET}}_{AB} e^{\Lambda^{\mathrm{ET}}_{AB} t} \mathcal{S}^{\mathrm{ET}\,-1}_{AB}, \tag{51}$$

where we have used the spectral decomposition of the projected reference Liouvillian

$$(\mathcal{L}^{AB}_0 + \tilde{\mathcal{V}}^{AB}_{\mathrm{ET}}) \mathcal{S}^{\mathrm{ET}}_{AB} = \Lambda^{\mathrm{ET}}_{AB} \mathcal{S}^{\mathrm{ET}}_{AB}, \tag{52}$$

where $\mathcal{L}^{AB}_0$ is defined as the block of $\mathcal{L}_0$ [as given in Eq. (42)] that acts solely on AB coherences, and likewise for $\tilde{\mathcal{V}}^{AB}_{\mathrm{ET}}$ [with $\tilde{\mathcal{V}}_{\mathrm{ET}}$ given in Eq. (45)], and $\mathcal{S}^{\mathrm{ET}}_{AB}$ is the matrix of eigenvectors and $\Lambda^{\mathrm{ET}}_{AB}$ is the diagonal matrix of eigenvalues. Due to the block diagonal structure of $\mathcal{L}^{AB}_0 + \tilde{\mathcal{V}}^{AB}_{\mathrm{ET}}$, this can be straightforwardly evaluated. The correlation function $G^{C}_{AB}(t)$ is given by

$$G^{C}_{AB}(t) = \mathrm{Tr}_{\mathrm{b_{CT}}}[e^{-i\hat{H}^{\mathrm{b_{CT}}}_{A} t/\hbar} e^{+i\hat{H}^{\mathrm{b_{CT}}}_{B} t/\hbar} \hat{\rho}^{\mathrm{b_{CT}}}_{C}], \tag{53}$$

which is the moment generating function for the energy gap between subsystems A and B, with $\hat{H}^{\mathrm{b_{CT}}}_{A}$ defined in Eq. (30). The remaining diagonal $\mathcal{R}^{\mathrm{ET}}_{AA}$ terms are given by

$$\mathcal{R}^{\mathrm{ET}}_{AA} = -\sum_{B\neq A} \left(\mathcal{L}^{\mathrm{L},BA}_{H_{\mathrm{ET}}} \mathcal{G}^{A}_{BA} \mathcal{L}^{\mathrm{L},BA}_{H_{\mathrm{ET}}} + \mathcal{L}^{\mathrm{R},AB}_{H_{\mathrm{ET}}} \mathcal{G}^{A}_{AB} \mathcal{L}^{\mathrm{R},AB}_{H_{\mathrm{ET}}} \right) \tag{54}$$

as required to conserve population.

For practical calculations, we use the full version of these expressions, but insight into the effect of ET on the exciton dynamics can be gained by making some additional approximations. First, we consider the limit where the system and LE bath time scales are long compared to the decay time of $G^{\mathrm{LE}}_{\mathrm{CT,LE}}(t)$. In this limit, the $\mathcal{R}^{\mathrm{ET}}_{\mathrm{LE,LE}}$ term becomes

$$\mathcal{R}^{\mathrm{ET}}_{\mathrm{LE,LE}} = -\sum_{n=1}^{N_{\mathrm{CT}}} \frac{k_{\mathrm{CT}_n\leftarrow\mathrm{LE}}}{2} \{\hat{P}_n, \cdot\} - \frac{i}{\hbar} \sum_{n=1}^{N_{\mathrm{CT}}} \Delta_n [\hat{P}_n, \cdot], \tag{55}$$

i.e., a sum of dissipative and conservative terms. Here, $k_{\mathrm{CT}_n\leftarrow\mathrm{LE}}$ is the Fermi's golden rule rate constant for ET from the LE manifold to the CT_n state,[55]

$$k_{\mathrm{CT}_n\leftarrow\mathrm{LE}} = \frac{|V_{\mathrm{CT}_n\leftarrow\mathrm{LE}}|^2}{\hbar^2} \int_{-\infty}^{\infty} G^{\mathrm{LE}}_{\mathrm{CT,LE}}(t) e^{-i(E_{\mathrm{CT}_n} - \tilde{E}_{\mathrm{LE}})t/\hbar}\, \mathrm{d}t, \tag{56}$$

and $\tilde{E}_{\mathrm{LE}}$ is an effective energy scale of the LE states such that $\hat{H}_{\mathrm{LE,s}} \approx \tilde{E}_{\mathrm{LE}} \hat{\Pi}_{\mathrm{LE}}$, $\hat{H}_{\mathrm{CT}_n,\mathrm{s}} = E_{\mathrm{CT}_n} \hat{\Pi}_{\mathrm{CT}_n}$, where the effective coupling constant

$$|V_{\mathrm{CT}_n\leftarrow\mathrm{LE}}|^2 = \sum_{m=1}^{N_{\mathrm{LE}}} |V_{\mathrm{LE}_m,\mathrm{CT}_n}|^2 \tag{57}$$

is given by a sum over couplings involving all of the LE states [as given in Eq. (7)]. Finally, $\hat{P}_n = |\psi_n\rangle\langle\psi_n|$ is a projection operator onto the reactive state in the LE manifold given by

$$|\psi_n\rangle = \frac{1}{|V_{\mathrm{CT}_n\leftarrow\mathrm{LE}}|} \sum_{m=1}^{N_{\mathrm{LE}}} |\mathrm{LE}_m\rangle V_{\mathrm{LE}_m,\mathrm{CT}_n} \tag{58}$$

and Δ_n is an energy shift term given by

$$\Delta_n = \frac{|V_{\mathrm{CT}_n\leftarrow\mathrm{LE}}|^2}{\hbar}\, \mathrm{Im} \int_0^\infty G^{\mathrm{LE}}_{\mathrm{CT,LE}}(t) e^{-i(E_{\mathrm{CT}_n} - \tilde{E}_{\mathrm{LE}})t/\hbar}\, \mathrm{d}t, \tag{59}$$

which in the limit of a highly activated reaction is given by

$$\Delta_n \approx \frac{|V_{\mathrm{CT}_n\leftarrow\mathrm{LE}}|^2}{\Delta E_{\mathrm{CT}_n\leftarrow\mathrm{LE}}}, \tag{60}$$

where $\Delta E_{\mathrm{CT}_n\leftarrow\mathrm{LE}}$ is the vertical energy gap from the LE state to the CT_n state.[56,58]

From this, we deduce that electron transfer has three main effects on the exciton dynamics. First, the ET causes population loss from the LE manifold from the reactive state $|\psi_n\rangle$. Second, it causes decoherence between the states $|\psi_n\rangle$ state and the rest of the manifold of LE states. Third, the energy shift terms perturb the exciton dynamics, modifying the energy gaps and couplings between LE states. If the reactive state is just a specific localized LE state, i.e., $|\psi_n\rangle = |\mathrm{LE}_{r_n}\rangle$, then the energy shift term just alters the energy of this LE state, which in the excitonic basis introduces coupling between delocalized excitonic states as well as shifting exciton state energies. In the limit of Gaussian statistics for the bath and high temperature, this reduces to Marcus theory.[55,76,77] Equation (56) ignores the effect of exciton formation, which shifts the free energy of states in the LE manifold, thereby changing the rate constants for electron transfer. The full hybrid HEOM/QME theory that we use in simulations, however, includes this important effect.

D. The radiative decay term

The radiative coupling terms can be derived in a similar manner to the ET term, the details of which are given in the Appendixes. Here, we simply state the final expressions for the two nonzero radiative transfer terms $\mathcal{R}^{\mathrm{R}}_{\mathrm{GS,LE}}$ and $\mathcal{R}^{\mathrm{R}}_{\mathrm{LE,LE}}$. The GS ← LE transfer term is given by

$$\mathcal{R}^{\mathrm{R}}_{\mathrm{GS,LE}} = \frac{1}{6\hbar\varepsilon_0 c_0^3 \pi} \sum_{\alpha=x,y,z} \left(\mathcal{L}^{\mathrm{L}}_{\alpha} \mathcal{S}^{0,\mathrm{s}}_{\mathrm{LE,GS}} \Omega^{3}_{\mathrm{LE,GS}} (\mathcal{S}^{0,\mathrm{s}}_{\mathrm{LE,GS}})^{-1} \mathcal{L}^{\mathrm{R}}_{\alpha} + \mathcal{L}^{\mathrm{R}}_{\alpha} \mathcal{S}^{0,\mathrm{s}}_{\mathrm{GS,LE}} \Omega^{3}_{\mathrm{GS,LE}} (\mathcal{S}^{0,\mathrm{s}}_{\mathrm{GS,LE}})^{-1} \mathcal{L}^{\mathrm{L}}_{\alpha} \right). \tag{61}$$

Similarly, the $\mathcal{R}^{\mathrm{R}}_{\mathrm{LE,LE}}$ term can be evaluated as

$$\mathcal{R}^{\mathrm{R}}_{\mathrm{LE,LE}} = -\frac{1}{6\hbar\varepsilon_0 c_0^3 \pi} \sum_{\alpha=x,y,z} \left(\mathcal{L}^{\mathrm{R}}_{\alpha} \mathcal{S}^{0,\mathrm{s}}_{\mathrm{LE,GS}} \Omega^{3}_{\mathrm{LE,GS}} (\mathcal{S}^{0,\mathrm{s}}_{\mathrm{LE,GS}})^{-1} \mathcal{L}^{\mathrm{R}}_{\alpha} + \mathcal{L}^{\mathrm{L}}_{\alpha} \mathcal{S}^{0,\mathrm{s}}_{\mathrm{GS,LE}} \Omega^{3}_{\mathrm{GS,LE}} (\mathcal{S}^{0,\mathrm{s}}_{\mathrm{GS,LE}})^{-1} \mathcal{L}^{\mathrm{L}}_{\alpha} \right), \tag{62}$$

where $\mathcal{L}^{\mathrm{L}}_{\alpha}\hat{\sigma} = \hat{\Pi}_{\mathrm{GS}} \hat{\mu}_{\alpha} \hat{\Pi}_{\mathrm{LE}} \hat{\sigma}$ and $\mathcal{L}^{\mathrm{R}}_{\alpha}\hat{\sigma} = \hat{\sigma} \hat{\Pi}_{\mathrm{LE}} \hat{\mu}_{\alpha} \hat{\Pi}_{\mathrm{GS}}$, where the dipole moment operators $\hat{\mu}_{\alpha}$ are given in Eq. (10). These expressions use the eigenvalue decompositions of the blocks of $\mathcal{L}_{0,\mathrm{s}}$, $\mathcal{L}^{\mathrm{GS,LE}}_{0,\mathrm{s}} = \mathcal{S}^{0,\mathrm{s}}_{\mathrm{GS,LE}} (i\Omega_{\mathrm{GS,LE}}) (\mathcal{S}^{0,\mathrm{s}}_{\mathrm{GS,LE}})^{-1}$, and $\mathcal{L}^{\mathrm{LE,GS}}_{0,\mathrm{s}} = \mathcal{S}^{0,\mathrm{s}}_{\mathrm{LE,GS}} (-i\Omega_{\mathrm{LE,GS}}) (\mathcal{S}^{0,\mathrm{s}}_{\mathrm{LE,GS}})^{-1}$, where $\Omega_{\mathrm{GS,LE}}$ and $\Omega_{\mathrm{LE,GS}}$ are diagonal matrices with real positive-valued entries. It should be noted that the decay rates for the excitonic states $|\epsilon_n\rangle$ appearing in these expressions exactly correspond to the standard Wigner–Weisskopf decay rates.[23]

IV. EXCITON DIMER MODEL

As a test for the approximations that go into the hybrid HEOM/QME method, we have performed simulations on a model exciton dimer, consisting of two LE states, coupled to a single CT state. The b_{CT} bath is taken to be harmonic in this example, allowing us to obtain exact dynamics directly with the HEOM method. The LE system Hamiltonian for this model is

$$\hat{H}_{\mathrm{LE,s}} = \frac{\Delta\epsilon}{2} |\mathrm{LE}_1\rangle\langle \mathrm{LE}_1| - \frac{\Delta\epsilon}{2} |\mathrm{LE}_2\rangle\langle \mathrm{LE}_2| + J(|\mathrm{LE}_1\rangle\langle \mathrm{LE}_2| + |\mathrm{LE}_2\rangle\langle \mathrm{LE}_1|) \tag{63}$$

and the CT state Hamiltonian is taken to be $\hat{H}_{\mathrm{CT,s}} = (\Delta E_{\mathrm{CT}} + \lambda_{\mathrm{CT}}) |\mathrm{CT}\rangle\langle \mathrm{CT}|$ and the CT bath shift operator is taken as $\Delta\hat{V}^{\mathrm{b_{CT}}}_{\mathrm{CT}} = \hat{B}_{\mathrm{CT}}$, where $\hat{B}_{\mathrm{CT}}$ is a harmonic bath displacement operator. The LE baths and the b_{CT} bath are taken to have Debye spectral densities[11]

$$\mathcal{J}_j(\omega) = \frac{\lambda_j}{2} \frac{\gamma_{\mathrm{D}}\omega}{\gamma_{\mathrm{D}}^2 + \omega^2}, \tag{64}$$

where $j = \mathrm{LE}_1, \mathrm{LE}_2$, or CT labels the bath. In this model, we set $\lambda_{\mathrm{LE}_1} = \lambda_{\mathrm{LE}_2} = \lambda_{\mathrm{LE}}$ and only the LE_2 state is coupled to the CT state with a coupling coefficient $V_{\mathrm{LE}_2,\mathrm{CT}} = V$. The correlation coefficients $\kappa^{\mathrm{CT}}_{\mathrm{LE}_n}$ describing the correlation between the CT state energy gap and the LE state energy gaps are taken to be $\kappa^{\mathrm{CT}}_{\mathrm{LE}_1} = 0$ and $\kappa^{\mathrm{CT}}_{\mathrm{LE}_2} = \kappa$. The structure of the coupling between states and the partitioning into different HEOM/QME hierarchies, $|\sigma_A(t)\rangle\rangle$, is illustrated in Fig. 3(a).

The HEOM/QME calculations were performed with the adaptive short iterative Arnoldi integrator described in the supplementary material of Ref. 78, with a Krylov subspace dimension of $k = 9$, and an error tolerance parameter of $\epsilon = 10^{-12}$. The hierarchy was truncated using the frequency cutoff criterion, with ADOs with $\gamma_{\mathbf{n}} > \Gamma_{\mathrm{c}} = 10\gamma_{\mathrm{D}}$ excluded from the hierarchy. The same cutoff scheme was used to truncate $\tilde{\mathcal{V}}$ in evaluating the electron transfer kernel but with a looser choice of cutoff parameter $\Gamma_{\mathrm{c,ET}} = 2.5\gamma_{\mathrm{D}}$, so overall couplings between only 6 of the 55 ADOs were accounted for in evaluating $\mathcal{R}^{\mathrm{ET}}_{AB}$. The HEOM was closed using the termination scheme and low temperature correction described in Ref. 78.

The exact HEOM calculations on the dimer model were also performed using the adaptive short iterative Arnoldi integrator with $k = 9$ and $\epsilon = 10^{-11}$. The problem was simplified by reducing the number of baths from three to two as described in Appendix B—this greatly reduced the number of ADOs needed in the exact calculations. The hierarchy was truncated using a reorganization energy weighted frequency cutoff scheme, wherein ADOs with a weight $w_{\mathbf{n}} = \sum_{jk} \nu_{jk} n_{jk}/\lambda_j > \tilde{L}_{\mathrm{c}}$ are excluded from the hierarchy, with $\tilde{L}_{\mathrm{c}} = 20$. This scheme accounts for the fact that the hierarchy needs to be deeper for the modes with of larger reorganization energy baths because coupling coefficients down the hierarchy scale as $a_{jk} \propto \sqrt{\lambda_j}$. This more efficiently truncates the HEOM than other schemes, such as the frequency cutoff scheme[20] or the L, M cutoff scheme.[73]

As a first example of the HEOM/QME method, we performed simulations for the dimer model with $\beta\hbar\gamma_{\mathrm{D}} = 0.25$, $\beta\Delta\epsilon = 1$, $\beta V = 0.1$, $\beta\lambda_{\mathrm{CT}} = 5$, $\kappa = 1$, and $\beta\Delta E_{\mathrm{CT}} = -6$ [labeled model A in Fig. 3(b)], with a range of values of λ_{LE} and J. The initial condition was set to $\hat{\sigma}_{\mathrm{LE}}(0) = |\mathrm{LE}_1\rangle\langle \mathrm{LE}_1|$ and $\hat{\sigma}_{\mathrm{CT}}(0) = 0$. We look at three regimes of the exciton dynamics: the damped coherent transport regime ($\beta\lambda_{\mathrm{LE}} = 0.1$ and $\beta J = 1$), the vibrationally assisted transport regime ($\beta\lambda_{\mathrm{LE}} = 1$ and $\beta J = 1$), and the incoherent Förster transport regime ($\beta\lambda_{\mathrm{LE}} = 0.1$ and $\beta J = 0.1$). These model parameters are chosen to be typical of coupled LE and CT states in light harvesting complexes such as the Chl*a* dimer coupled to lutein in Fig. 1.[21]

In Fig. 3(b), we compare the exact simulated dynamics to the hybrid HEOM/QME dynamics, looking at three observables: the total LE state population, $p_{\mathrm{LE}}(t)$, the relative population difference between the LE states, $(p_{\mathrm{LE}_1}(t) - p_{\mathrm{LE}_2}(t))/p_{\mathrm{LE}}(t)$, and the relative LE coherence, defined as $2\,\mathrm{Re}[\langle \mathrm{LE}_1|\hat{\sigma}_{\mathrm{LE,s}}(t)|\mathrm{LE}_2\rangle]/p_{\mathrm{LE}}(t)$. We see that in this example, the hybrid HEOM/QME method performs remarkably well in the three regimes of exciton dynamics, with only small deviations in the long time limits of the relative LE population differences and coherences. In particular, the time scale of decay of the LE population is captured very well by the hybrid method for all three models.

In a second, more challenging, test for the hybrid method, we performed simulations for the same dimer model with $\beta\hbar\gamma_{\mathrm{D}} = 1.75$, $\beta\Delta\epsilon = 1$, $\beta V = 0.5$, $\beta\lambda_{\mathrm{CT}} = 5$, $\kappa = 1$, and $\beta\Delta E_{\mathrm{CT}} = -2$ [labeled model B in Fig. 3(b)]. In this example, the coupling between the CT and the LE manifold is much larger, the free energy of the CT state is higher, so back reaction effects are more significant. Furthermore, the characteristic bath frequency is comparable now to the LE system frequencies, leading to significant non-Markovian effects in

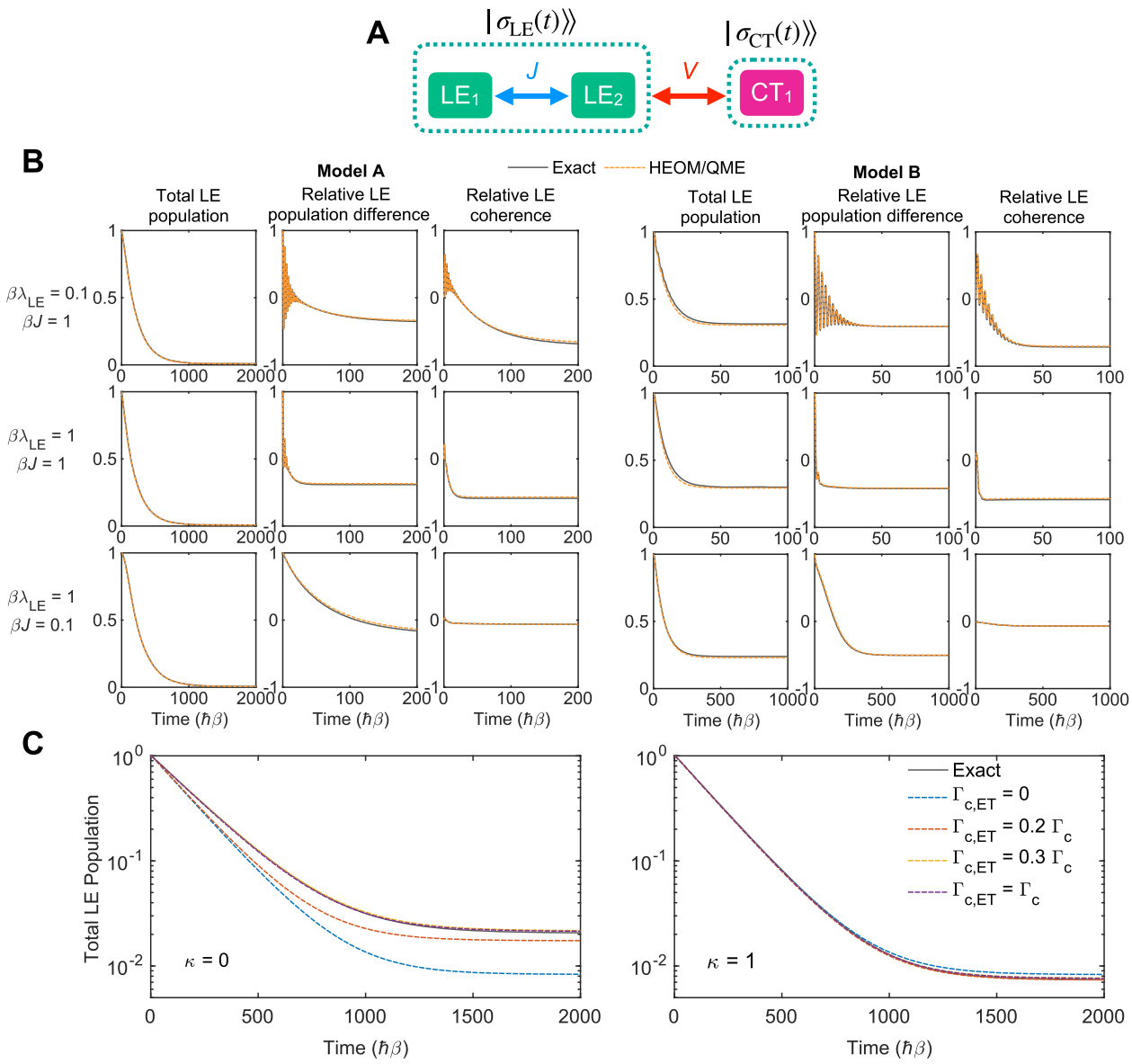

FIG. 3. (a) Schematic diagram showing the LE states and CT state in the dimer model, and the nonzero interstate couplings, together with the partitioning into reduced hierarchies. (b) A comparison of the hybrid HEOM/QME method with the exact HEOM result for the dimer model A with $\beta\hbar\gamma_D = 0.25$, $\beta\Delta\epsilon = 1$, $\beta V = 0.1$, $\beta\lambda_{CT} = 5$, $\kappa = 1$, and $\beta\Delta E_{CT} = -6$ (left three columns) and for the dimer model B with $\beta\hbar\gamma_D = 1.75$, $\beta\Delta\epsilon = 1$, $\beta V = 0.5$, $\beta\lambda_{CT} = 5$, $\kappa = 1$, and $\beta\Delta E_{CT} = -2$ (right three columns), with a range of values of λ_{LE} and J. The first and fourth columns show the total LE population dynamics, the second and fifth columns show the LE population difference relative to the total LE population, and the third and sixth columns show the real part of the LE coherence relative to the total LE population. The rows correspond to models with $\beta J = 1, \beta\lambda_{LE} = 0.1$ (top), $\beta J = 1, \beta\lambda_{LE} = 1$ (middle), and $\beta J = 0.1, \beta\lambda_{LE} = 1$ (bottom). (c) Convergence of the hybrid HEOM/QME results with respect to $\Gamma_{c,ET}$ with parameters described in the text. The panels correspond to $\kappa = 0$ (left) and $\kappa = 1$ (right).

the LE dynamics, and the ET rate from the LE manifold to the CT state is closer to the frequencies of exciton dynamics. However, in Fig. 3(a), we see that the hybrid method still performs well in all regimes of exciton dynamics, with only small errors in the decay of the total LE population. The errors in the population dynamics can likely be attributed to the increased importance of CT-LE coherence in this example, which is treated with a perturbative-Markovian approximation with the hybrid method. Within high temperature perturbation theory, the steady state average CT-LE coherence scales roughly as $V/\lambda_{CT} = 0.1$, which is five times larger in this set of

models compared to the previous ones with $V/\lambda_{CT} = 0.02$, so it is not unexpected that the rate of ET is not captured quite as well in these more challenging models.

As a final example, we examine the convergence of the LE population dynamics with respect to the cutoff parameter $\Gamma_{c,ET}$, for $\kappa = 0$ and $\kappa = 1$. When $\kappa = 1$, there is no contribution from the b_{LE_2} bath to the free energy change or reorganization energy of the charge transfer process; however, when $\kappa = 0$, the b_{LE_2} bath reorganizes in the $LE_2 \rightarrow CT$ transfer, which means that when $\kappa = 0$, this bath has a significant contribution to the free energy change and reorganization energy of the $LE_2 \rightarrow CT$ process. In these simulations, we set $\Gamma_c = 7\gamma_D$ and examine the population dynamics for $\beta\lambda_{LE} = 1$, $\beta J = 1$ with model parameters the same as in dimer model A [as in Fig. 3(b)]. In Fig. 3(c), we show the population dynamics for various $\Gamma_{c,ET}$ values for $\kappa = 0$ and $\kappa = 1$. We see that convergence is much faster in the $\kappa = 1$ case, where the LE bath does not contribute to the reorganization energy or free energy change of the $LE \rightarrow CT$ process, so only the LE system energies need to be accounted for in the kernel to obtain accurate results. Conversely, when $\kappa = 0$, there is a significant contribution to the reorganization energy and free energy change from the LE bath (roughly 20%); therefore, the LE bath response has to be accounted for in more detail in the ET kernel to obtain accurate results.

V. LHCII

Having established the accuracy of the hybrid HEOM/QME method on a range of dimer models, we turn to a more complex problem, charge transfer energy quenching in LHCII. LHCII is an important light harvesting complex in plants, which absorbs light energy and transports it to reaction centers.[1] It is also known to play a role in non-photochemical quenching in plants, and one mechanism for excitation energy quenching in the complex is electron transfer from the carotenoid lutein to excited chlorophyll-*a* molecules.[6,8,67,79] The resulting $Chla^{\bullet-}Lut^{\bullet+}$ pairs recombine to the ground state of the system, thereby quenching excitation energy as heat. In Ref. 67, Cupellini *et al.* parameterized the free energy change, reorganization energy, and diabatic coupling for charge transfer from Lut1 to $a612^*$ and Lut2 to $a603^*$; from this, they used Marcus theory and a simple kinetic model to estimate the excitation lifetime of chlorophyll in LHCII. This model treated the coupled $Chla^*$ and $Chlb^*$ dynamics with a simple kinetic model, where EET between the $a612^*$ and $a603^*$ states and the pool of $Chla^*$ states is modeled as a simple first order rate process. This treatment ignores many of the details of EET in LHCII, such as the strong coupling between the $a612^*$ and $a611^*$ states, and the $a603^*$ and $a602^*$ states, which leads to exciton formation.

A. Model details

In order to go beyond a simple kinetic treatment of excitation energy transfer and CT quenching in LHCII, we have modeled the coupled exciton and charge transfer dynamics of an LHCII monomer with the hybrid HEOM/QME method. This allows us to fully explore the effects of coupled exciton and charge transfer dynamics on the Chl^* lifetime. The LHCII monomer contains eight Chl*a* and six Chl*b* molecules, excitations on which are all coupled, together with two lutein molecules (Lut1 and Lut2), as shown in Fig. 4(a). We partition the system into an LE space, two CT states, and the GS as outlined in Fig. 4(b). We explore this system using two different LE Hamiltonians for LHCII, which have been parameterized using various spectroscopic data: the model of Müh *et al.* from Ref. 66 (henceforth referred to as model 1) and the model of Novoderezhkin *et al.* from Ref. 46 (henceforth referred to as model 2). These models differ subtly in their $Chla^*$ and $Chlb^*$ site energies and couplings, which is shown below to have a significant effect on the quenching dynamics. The LE–environment coupling is treated with the HEOM approach, with a single Debye bath for each site, with a reorganization energy of 220 cm^{-1} and characteristic frequency, γ_{D,Chl^*}, of 353.7 cm^{-1}, as taken from the study of Kreisbeck *et al.* in Ref. 21. This model for the LE–environment coupling misses some small vibrational resonance effects in the $Chlb^*$ to $Chla^*$ energy transfer dynamics and it cannot reproduce structured vibrational features in the monomer absorption spectrum, but it does accurately capture the important features of the excitation energy dynamics when compared with more complex structured environment models.[21] Because we are primarily interested in time scales of excitation energy redistribution and quenching in this system, and because we wish to use as simple a spectral density as possible to reduce the number of baths needed in the HEOM calculations, we choose to use this spectral density for the Chl^* excitations.

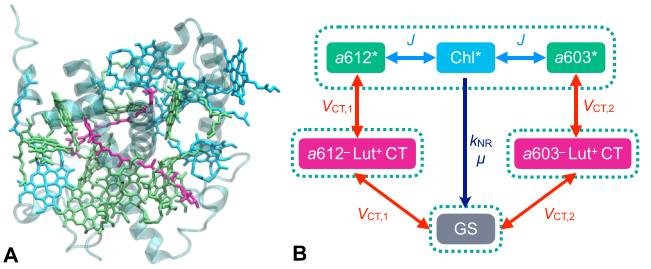

FIG. 4. (a) Structure of the LHCII monomer (PDB 1RWT chain C[68]) showing the chlorophyll A (green), chlorophyll B (light blue), and lutein (pink) molecules. (b) A scheme of the electronic states and couplings used in this model. Couplings between states are represented by double-headed arrows, the single-headed arrow represents the radiative and non-radiative transfer processes, and the dashed lines represent the blocks of states treated with their own explicit hierarchies of ADOs $|\sigma_A(t)\rangle\rangle$.

In order to describe the charge transfer process, we use the reorganization energies, charge transfer free energy changes, and diabatic couplings calculated by Cupellini *et al.* from QM/MM (quantum mechanics/molecular mechanics) simulations. The reorganization energy for the b_{CT} bath for each charge recombination process to the GS is assumed to be the same as for the corresponding charge separation, which is a reasonable assumption if polarization of the environment and lutein reorganization are the dominant contributions to the total reorganization energy, and the free energy of the GS relative to the excited states is taken from the LE model Hamiltonians. Using these parameters, we assume the b_{CT} bath can be treated as harmonic, with a Debye spectral density of $\gamma_D = 30$ cm^{-1}, which is representative of the response of the polarizable environment.[80] We have also explored how adding

structure to this spectral density affects the quenching dynamics as will be explained below. For the Lut1 → $a612^*$ charge transfer and Lut2 → $a603^*$ charge transfer, we used the same diabatic coupling matrix elements as calculated by Cupellini *et al.*,[67] denoted as V_{CT1} and V_{CT2}, respectively. We use the same diabatic couplings for the recombination processes $a612^- \rightarrow \text{Lut1}^+$ and $a603^- \rightarrow \text{Lut2}^+$, given that the donor–acceptor separation is the same for the charge separation and charge recombination steps, although a different Chl*a* orbital is involved in the recombination process, so the couplings will be different in reality. The full set of parameters and the LE state Hamiltonians are given in Appendix D.

The transition dipole moment operators for the LE system are calculated using the atomic positions from PDB 1RWT[68] for the Chl*a* and Chl*b* molecules and assuming the transition dipole moment for each LE state, $\boldsymbol{\mu}_n$, points in the direction from N_B to N_D.[81] The magnitude of the transition dipole moment operator is taken to be 4.0 D for Chl*a* and 3.4 D for Chl*b*.[23] In modeling excitation relaxation in the LHCII monomer, it is also necessary to incorporate direct internal conversion of the Chla^* and Chlb^* states. This was done by adding the following non-radiative transition operators to the HEOM/QME:

$$\mathcal{R}^{\text{NR}}_{\text{LE,LE}}\,\hat{\sigma}_{\text{LE},\mathbf{n}}(t) = -\sum_{n=1}^{N_{\text{LE}}} \frac{k_{\text{NR},n}}{2}\{|\text{LE}_n\rangle\langle\text{LE}_n|, \hat{\sigma}_{\text{LE},\mathbf{n}}(t)\}, \tag{65}$$

$$\mathcal{R}^{\text{NR}}_{\text{GS,LE}}\,\hat{\sigma}_{\text{LE},\mathbf{n}}(t) = \sum_{n=1}^{N_{\text{LE}}} k_{\text{NR},n}|\text{GS}\rangle\langle\text{LE}_n|\,\hat{\sigma}_{\text{LE},\mathbf{n}}(t)|\text{LE}_n\rangle\langle\text{GS}|, \tag{66}$$

and we set $k_{\text{NR},n} = 0.25\ \text{ns}^{-1}$, in line with the kinetic model of Cupellini *et al.*[67] A similar model has been used previously in quantum master equation-based studies of the bacterial LHI/LHII system,[81] and a justification of this form of the non-radiative transition operator from the Nakajima–Zwanzig equation is given in Appendix C.

In all simulations with the hybrid HEOM/QME method, we use an adaptive short iterative Arnoldi integrator (as described in Ref. 78) with an error tolerance parameter of 10^{-8} and Krylov subspace dimension of 16. The Nakajima–Zwanzig low temperature and termination corrections described in Ref. 78 were also used in these simulations, and using this scheme, the populations of Chla^*, Chlb^* and CT states were found to be converged with an HEOM frequency cutoff parameter of $\Gamma_c = 3\gamma_{\text{D,Chl}^*}$ using the Matsubara decomposition scheme for the correlation functions. The cutoff parameter for the ET kernels was set to $\Gamma_{c,\text{ET}} = 2\gamma_{\text{D,Chl}^*}$ for the charge separation steps and $\Gamma_{c,\text{ET}} = 0$ for the charge recombination steps. All simulations were run at a temperature of 300 K. These methods are all implemented in the freely available HEOM-lab code,[82] which was used to perform all simulations presented in this paper.

B. Population dynamics

As a first application of the hybrid HEOM/QME method to LHCII charge transfer quenching, we have simulated the population dynamics for the Chla^*, Chlb^*, and CT states for Model 1, with the initial condition set as an excitation completely localized on *a*612. The population dynamics are shown in Fig. 5. For this initial condition, there is an early rapid transfer of population to the strongly coupled $a611^*$ state, as an exciton is formed where the

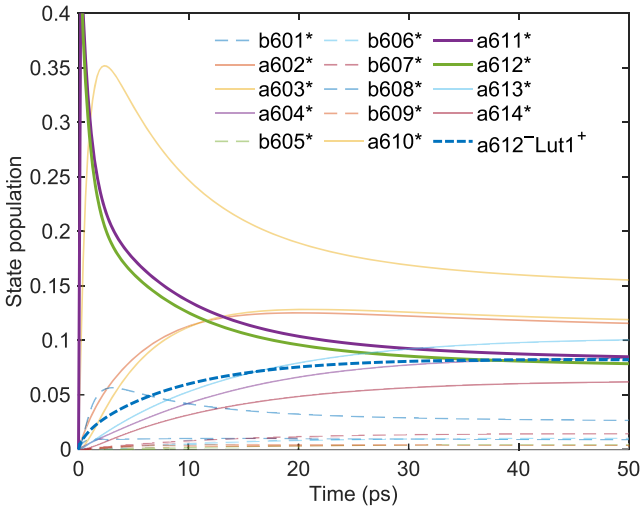

FIG. 5. Populations of the LE states and the $a612^-\text{Lut1}^+$ state calculated with the hybrid HEOM/QME method for an initial excitation localized on *a*612 using the Model 1 LE Hamiltonian.

excitation is delocalized between the two Chl*a* sites. This exciton formation is followed by slower excitation energy transfer to the other Chla^* and Chlb^* states as well as the $a612^-\text{Lut1}^+$ state. Importantly, formation of the $a612^-\text{Lut1}^+$ state from the exciton state happens on a comparable time scale, roughly 10 ps, to energy redistribution between the Chla^* and Chlb^* states, highlighting the need to treat both the CT and exciton dynamics simultaneously. We found that at least $\Gamma_c = 3\gamma_{\text{D,Chl}^*}$ was needed to converge the population dynamics, with hierarchy termination corrections from Ref. 78, corresponding to treating the exciton system–environment coupling up to sixth order in non-Markovian perturbation theory, with partial Markovian eighth-order corrections. As has been demonstrated previously by Kreisbeck *et al.*[21] for LHCII in the absence of CT quenching, simple mixed Redfield–Förster theories cannot describe the population dynamics of this system without *a posteriori* tuning of domain definitions. In contrast, the population dynamics from the HEOM/QME do not require such *a posteriori* fine-tuning and instead can be systematically converged by increasing the size of the hierarchy. Direct HEOM calculations on this system would, however, not be feasible. A rough estimate of the depth of hierarchy needed for a system treating b_{CT} with the HEOM explicitly can be obtained by requiring that the termination correction term proposed in Ref. 78 is small compared to the $\gamma_{\mathbf{n}}$ in the terminating ADO. From this, we find that the hierarchy depth, L, would need to satisfy $L > 2\lambda_{\text{CT}}/(\beta\gamma^2_{\text{D,CT}}) \approx 2500$. As a result, this calculation would be intractable with standard HEOM methods due to the very large reorganization energy associated with the charge transfer processes; but, with the hybrid HEOM/QME method, this calculation runs in a few minutes on a single central processing unit (CPU).

In order to compare the kinetic model used by Cupellini *et al.* to our model including the full exciton dynamics, we have also simulated the population dynamics where population is evenly divided between the Chla^* states, with no initial coherences between sites.

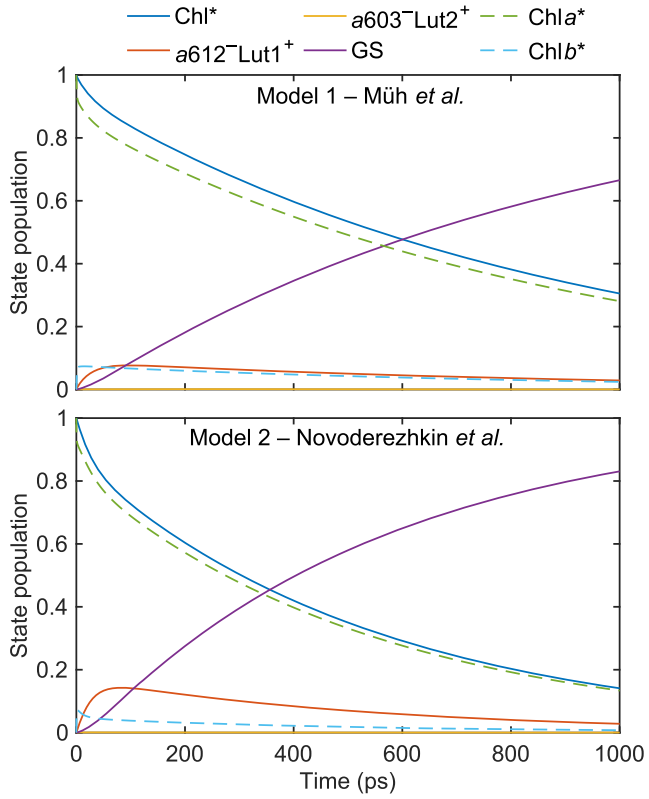

FIG. 6. Excited state population dynamics for LHCII with an initial excitation partitioned equally between all eight Chl*a** states with no coherences between these states, calculated with the hybrid HEOM/QME method. Results in the top panel use the Model 1 LE Hamiltonian and results in the bottom panel use the Model 2 LE Hamiltonian.

The total populations of the Chl*, Chl*a**, Chl*b**, and CT states and GS are shown for both models in Fig. 6. In both models, there is rapid equilibration between the Chl*a** and Chl*b** states, occurring on a time scale of a few picoseconds, followed by population transfer to the CT states within ten picoseconds. The $a612^{-}\text{Lut1}^{+}$ state is populated to a much greater extent than the $a603^{-}\text{Lut2}^{+}$ state because the latter lies nearly 1000 cm^{-1} above the Chl*a** states, whereas the former is nearly degenerate with the Chl*a** states. In Model 1, we observe a greater extent of population transfer to the Chl*b** states and a lesser extent of population transfer of the $a612^{-}\text{Lut1}^{+}$ state compared to that of Model 2.

Interestingly, the overall decay of the Chl* population is noticeably faster in Model 2 compared to Model 1. In order to quantify the excitation lifetime, we fit these population decay curves to a sum of three exponentials [constrained such that $p_{\text{Chl}^*}(t=0)=1$], and use this to calculate the integrated lifetime $\tau_{\text{eff}} = \int_0^\infty p_{\text{Chl}^*}(t)\,\mathrm{d}t$. For Model 1 we obtain $\tau_{\text{eff}} = 0.83$ ns and Model 2 we find $\tau_{\text{eff}} = 0.50$ ns.

Both these lifetime estimates are closer to the experimental value for the excitation lifetime, 2 ns for LHCII in a membrane, than that of the kinetic model of Cupellini *et al.*, which predicted a 0.3 ns integrated lifetime. This suggests the importance of treating the exciton dynamics explicitly in modeling charge transfer quenching in light harvesting complexes. We suspect that a significant source of error in our model, compared to experiment, is the estimate for the diabatic coupling for the charge recombination steps, which affects the lifetime of the CT states and, therefore, also strongly influences the CT quenching rate.

Part of the difference between the kinetic model of Cupellini *et al.* and our model is that we correctly account for exciton formation in the excited state dynamics, which changes the rate of population transfer from the LE manifold to the CT states. This is because exciton formation modifies the effective coupling matrix element by $\sim 1/\sqrt{2}$ for the charge transfer rate since charge transfer occurs from the excitonic state $|\psi\rangle \approx (1/\sqrt{2})(|a611^*\rangle - |a612^*\rangle)$ (although this picture is complicated by the LE bath reorganization, which reduces the relative coherence between the $a611^*$ and $a612^*$ states to ~0.16 for Model 1 and ~0.20 for Model 2, an effect that mixed Redfield–Förster theories would struggle to capture). Furthermore, exciton formation lowers the free energy of the initial excitonic state by ~100 cm^{-1} for both models. This means the effective free energy change for the formation of the $a612^{-}\text{Lut1}^{+}$ is ~0 cm^{-1}, which is reflected in Fig. 5, where the $a611^*$, $a612^*$, and $a612^{-}\text{Lut1}^{+}$ states have approximately equal population by $t = 50$ ps. This means the excitonic state is stabilized relative to the CT state and this decreases the steady state CT population, decreasing the rate of charge separation.

The faster quenching in Model 2 is primarily due to the larger steady state population of the $a612^{-}\text{Lut1}^{+}$ state, which provides the main channel for charge transfer quenching of the Chl* excitations. The larger steady state population of the $a612^{-}\text{Lut1}^{+}$ state can be explained by the differences between the excitonic structure of the two LHCII models. In Model 1, the *a*611-*a*612 excitonic state is the third lowest energy state, lying more than $k_B T$ above the lowest lying excitonic state, whereas in Model 2, the *a*611-*a*612 excitonic state is the lowest energy state, with the next nearest excitonic state lying about $0.5 k_B T$ above this. This means that in Model 2, more of the Chl*a** excitations are funneled into the excitonic state coupling to the quenching state, which leads to a greater extent of CT state formation and faster Chl* population decay. This illustrates the importance of the excitonic energy funnel in determining the quenching efficiency. This observation was not found to depend on the choice of spectral density for the LE coupling baths.

C. Role of the excitation energy funnel

In order to further explore the effects of the excitonic energy funnel on excitation quenching in LHCII, we have performed simulations on modified versions of the Model 1 and Model 2 Chl* Hamiltonians. For both models, we introduced a shift to the site energies of all states in the LE manifold except the *a*611 and *a*612 states, such that the site energies are changed from E_n to $E_n + \delta E$. The energy of the $a603^{-}\text{Lut2}^{+}$ charge transfer is shifted by the same amount. This effectively preserves the *a*611-*a*612 exciton state in the LE manifold but just shifts its energy relative to the remaining excitonic states. Varying the shift from −500 to +500 cm^{-1}, we have calculated the total Chl* population decay and the integrated lifetime from the population dynamics to quantify the changes to the Chl* excitation lifetime as shown in Fig. 7.

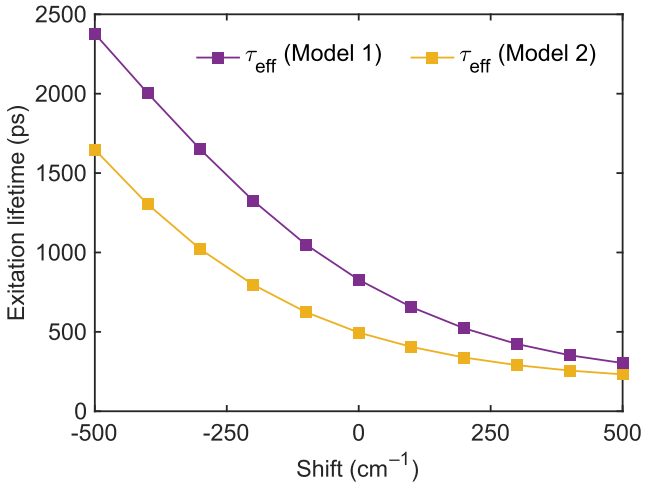

FIG. 7. τ_{eff} and τ_{max} for models 1 and 2 as a function of the local excitation energy shift as described in the text.

We see that for modified versions of both Model 1 and Model 2, shifts in the Chl* site energies can have a very large effect on the population dynamics and excitation lifetime. In particular, for Model 1, a change in shift from −200 to +200 cm^{-1} can change the excitation lifetime by more than a factor of 2. These significant changes in excitation lifetime for modest shifts in the excitation energies suggest a potential mechanism for the activation of non-photochemical quenching by changes in the energy funnel in light harvesting complexes directing excitations toward quenching sites.

D. Role of the charge transfer spectral density

We have examined the potential role of nuclear quantum effects in determining the charge transfer quenching lifetime. We modify the spectral density for the charge transfer processes to include an underdamped Brownian oscillator contribution,[11] where the new spectral density is

$$\mathcal{J}_{CT}(\omega) = (1-\alpha)\,\mathcal{J}_{D}(\omega) + \alpha\,\mathcal{J}_{BO}(\omega), \tag{67}$$

$$\mathcal{J}_{BO}(\omega) = \frac{\lambda}{2}\frac{\gamma\Omega^2\omega}{(\omega^2-\Omega^2)^2+\gamma^2\omega^2}, \tag{68}$$

where the first portion is a Debye spectral density with $\omega_D = 30$ cm^{-1}, which represents the low frequency environment contribution, and $\mathcal{J}_{BO}(\omega)$ models the high frequency contribution from C=C stretches in the lutein molecules.[83] In what follows, we have set $\Omega = 1500$ cm^{-1} and $\gamma = 50$ cm^{-1}, and we keep the total reorganization energy for each charge transfer process fixed at the values determined by Cupellini *et al.* We have varied the α parameter, which controls the spectral distribution of the reorganization energy, between 0 and 0.5 for the Model 1 exciton Hamiltonian, and for each value of α, we have simulated the population dynamics and calculated τ_{eff} and τ_{max}, again from an initial condition, where all Chla^* states are equally populated with no coherences.

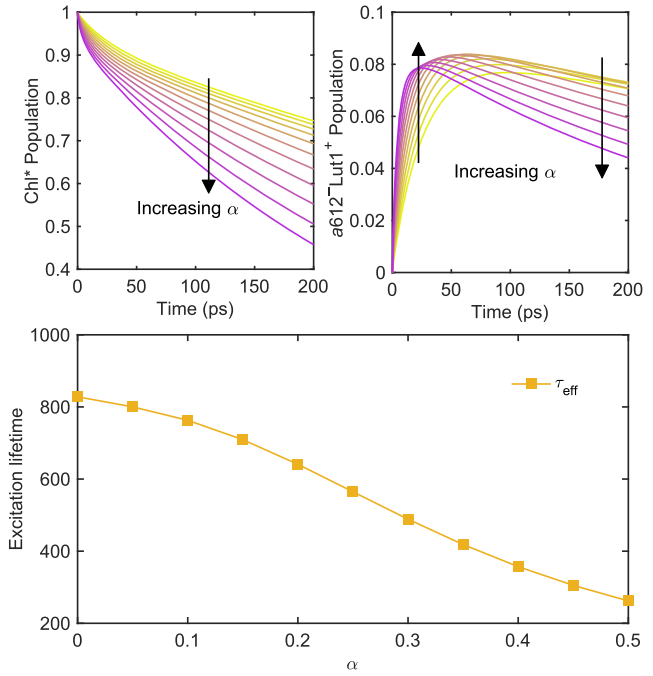

FIG. 8. Top left: Chl* population dynamics varying α from 0 (yellow) to 0.5 (purple). Top right: $a612^-Lut1^+$ population dynamics varying α (same color scheme as top left). Bottom: excitation lifetime as a function of α. All calculations use the Model 1 LE Hamiltonian with equally populated Chla^* states with no coherences as the initial condition.

The calculated total Chl* and $a612^-Lut1^+$ population dynamics are shown in the top panels of Fig. 8. We see that increasing the contribution to the charge transfer spectral density from the underdamped, high frequency Brownian oscillator decreases the lifetime of the Chl* excitations. The increased Brownian oscillator contribution increases the extent of nuclear quantum tunneling, which increases both the rate of charge separation and charge recombination. The effect of increasing the rates of both processes can be seen more clearly in the $a612^-Lut1^+$ population dynamics. At short times, as α increases, the rate of population transfer from the Chl* manifold to the $a612^-Lut1^+$ state increases due to an increasing charge separation rate, which transiently increases the quenching rate. At longer times, when the Chl* states and CT states have reached a steady state, increasing α increases the rate of decay of the $a612^-Lut1^+$ state, which arises due to an increased charge recombination rate with increasing α.

VI. DISCUSSION

Using the hybrid HEOM/QME method developed in this paper, we have been able to explore the charge transfer quenching dynamics in a LHCII monomer. Using previously parameterized models of excitation energy transfer and electron transfer in the LHCII pigment–protein complex, together with some physically motivated assumptions, we can obtain estimates of the excitation

lifetime closer to experimental values than those obtained using simple kinetic models.[67] The lifetime estimate, however, depends strongly on the model of local excitation energies and couplings used to describe the excitation energy transfer preceding charge transfer quenching. This may have interesting implications for the understanding of non-photochemical quenching processes in light harvesting complexes. It is generally assumed that non-photochemical quenching is activated by conformational changes, induced by pH changes or chemical modifications of the protein or bound carotenoids, in protein–pigment complexes moving quenchers into positions where they can efficiently couple to chromophores,[6,7,79,84–87] thereby increasing the rate of charge transfer quenching and/or excitation energy transfer quenching. The work here highlights the potential role of the excitation energy funnel in CT quenching, and we suggest that non-photochemical quenching could also be activated by changes in the site energies and couplings within the chromophore excited state manifold that funnel excitations toward quenching sites. These energy and coupling shifts could also be induced by conformational changes in the protein–pigment complex and could occur simultaneously with the conformational changes that move quenchers closer to chromophores. In this way, the energy funneling mechanism could work cooperatively with quenching activation by movement of quenchers. Interestingly, it has recently been found in one computational study that pH changes, which are believed to play a role in activating non-photochemical quenching, can create modest shifts in the Chl excitation energies in LHCII.[88]

Our exploration of the charge transfer spectral density has also highlighted the importance of understanding all details of charge transfer processes in light harvesting complexes, including the details of recombination processes and nuclear quantum effects. One particularly important factor for predicting charge transfer quenching rates is the rate of charge recombination from the CT state back to the electronic ground state of the system, which is strongly dependent on nuclear quantum effects as well as the energetics of charge recombination and the diabatic coupling strength. This is because the reverse electron transfer is often deep in the Marcus inverted regime; for example, in LHCII, the Lut-Chl*a* recombination processes have a free energy change of $-\Delta G \approx 3\lambda$, where nuclear tunneling effects play a decisive role in determining electron transfer rates.[89] Although in our study of LHCII, we have assumed that the electron transfers can be treated with a spin-boson mapping,[27] the theory developed here does not rely on this assumption. The correlation functions needed to evaluate the ET kernels, $G^C_{AB}(t)$, can be evaluated using various approximations including anharmonicity in the potential energy surfaces.[55,90–94] For example, $G^C_{AB}(t)$ could be evaluated classically[55] or using analytic continuation together with path integral methods to incorporate anharmonic nuclear quantum effects.[93]

In this work, we have assumed that we can treat the weakly and strongly coupled environments (corresponding to the EM field and b_{CT} degrees of freedom, respectively) as Markovian, but it may be possible to extend this treatment to non-Markovian cases by incorporating memory effects via the generalized quantum master equation[63–65] or via a time-convolutionless approach.[95] We also note that the framework of Zwanzig projection could be used to perturbatively treat effects of environment degrees of freedom other than b_{CT} and EM field degrees of freedom while retaining an exact hierarchical treatment of important non-Markovian bath modes.

VII. CONCLUDING REMARKS

In this paper, we have outlined how to rigorously combine the hierarchical equations of motion method with quantum master equations in both the strong system–bath coupling and weak system–bath coupling limits to model simultaneous excitation energy transfer and charge transfer in protein–pigment complexes. The hybrid HEOM/QME approach is based on the application of Zwanzig projection to derive a system of equation for a hierarchy of auxiliary density operators for the various electronic state manifolds. This method has been tested against numerically exact results for an excitonic dimer coupled to a charge transfer state, where it was found to yield accurate population and coherence dynamics across a range of excitation energy transfer regimes. We then applied the method to study charge transfer quenching in LHCII—a process suspected to play an important role in photoprotection in plants.

Using the hybrid HEOM/QME approach, we have been able to study the interplay of excitation energy transfer and charge transfer quenching in a realistic model of LHCII. Our results highlight the importance of the excitation energy funnel in determining quenching efficiency in protein–pigment complexes as well as the role of the CT state recombination rate when back electron transfer to reform LE states from CT states occurs at an appreciable rate as is the case in LHCII. We expect that the energy funnel mechanism could play a role in the activation of non-photochemical quenching in many systems and that it could occur cooperatively with other non-photochemical quenching (NPQ) activation mechanisms.

All the parameters needed in the hybrid HEOM/QME model can be obtained using well-established methods: For example, exciton Hamiltonians can be fit based on spectroscopic data[46,66] or using QM/MM simulations of protein–pigment complexes.[96] Likewise, electron transfer model parameters can be obtained using molecular dynamics simulations.[27,92] By combining existing computational tools with the hybrid HEOM/QME method, currently implemented in the freely available Matlab code HEOM-lab,[82] it may be possible to shed light on the precise mechanisms that produce non-photochemical quenching in photosynthetic organisms,[6] for example, how chemical modifications of carotenoids in the xanthophyll cycle activate NPQ in LHCII and related proteins like LHCX1.[7,84] For this reason, we anticipate the method to become a useful tool in studying non-photochemical quenching and reaction center processes in photosynthetic systems.

ACKNOWLEDGMENTS

T.P.F and D.T.L. acknowledge the support provided by the U.S. Department of Energy, Office of Science, Basic Energy Sciences, CPIMS Program Early Career Research Program under Award No. DE-FOA0002019.

AUTHOR DECLARATIONS

Conflict of Interest

The authors have no conflicts to disclose.

Author Contributions

Thomas P. Fay: Conceptualization (equal); Investigation (equal); Methodology (equal); Software (equal); Writing – original draft (equal); Writing – review & editing (equal). **David T. Limmer**: Conceptualization (equal); Funding acquisition (equal); Supervision (equal); Writing – review & editing (equal).

DATA AVAILABILITY

The data that support the findings of this study are available from the corresponding author upon reasonable request.

APPENDIX A: THE RADIATIVE DECAY TERM

We evaluate the radiative coupling term in the hybrid HEOM/QME in much the same way as the ET coupling term. Here, we assume that only the LE states and the GS are connected by the dipole moment operator, which means we only have to evaluate $\mathcal{R}^{\mathrm{R}}_{\mathrm{GS,LE}}$ and $\mathcal{R}^{\mathrm{R}}_{\mathrm{LE,LE}}$. Starting with $\mathcal{R}^{\mathrm{R}}_{\mathrm{GS,LE}}$, we can insert the dipole coupling term into the second order kernel and directly evaluate the radiative coupling term as

$$\begin{aligned}\mathcal{R}^{\mathrm{R}}_{\mathrm{GS,LE}} = \frac{1}{2\hbar\mathcal{V}_0\,\varepsilon_0}\sum_{\boldsymbol{k},p}\int_0^\infty \mathrm{d}t\,\omega_{\boldsymbol{k}} \\ \times\Big(\mathcal{L}^{\mathrm{L}}_{\boldsymbol{k}p}e^{\mathcal{L}_{0,\mathrm{s}}t}\mathcal{L}^{\mathrm{R}}_{\boldsymbol{k}p}\left\langle a_{\boldsymbol{k}p}(0)a^\dagger_{\boldsymbol{k}p}(t)\right\rangle_{\mathrm{b_{EM}}} \\ + \mathcal{L}^{\mathrm{R}}_{\boldsymbol{k}p}e^{\mathcal{L}_{0,\mathrm{s}}t}\mathcal{L}^{\mathrm{L}}_{\boldsymbol{k}p}\left\langle a_{\boldsymbol{k}p}(0)a^\dagger_{\boldsymbol{k}p}(t)\right\rangle^*_{\mathrm{b_{EM}}}\Big),\end{aligned} \tag{A1}$$

where we have assumed that we can approximate $\mathcal{L}_0 + \mathcal{V} \approx \mathcal{L}_{0,\mathrm{s}}$ in evaluating this term. The operators $\mathcal{L}^{\mathrm{L/R}}_{\boldsymbol{k}p}$ are given by

$$\mathcal{L}^{\mathrm{L}}_{\boldsymbol{k}p}\hat{\sigma} = i\hat{\Pi}_{\mathrm{GS}}(\hat{\boldsymbol{\mu}}\cdot\boldsymbol{e}_{\boldsymbol{k}p})\hat{\Pi}_{\mathrm{LE}}\hat{\sigma}, \tag{A2}$$

$$\mathcal{L}^{\mathrm{R}}_{\boldsymbol{k}p}\hat{\sigma} = -i\hat{\sigma}\hat{\Pi}_{\mathrm{LE}}(\hat{\boldsymbol{\mu}}\cdot\boldsymbol{e}_{\boldsymbol{k}p})^\dagger\hat{\Pi}_{\mathrm{GS}}, \tag{A3}$$

and the EM field operator correlation function can be evaluated as

$$\left\langle a_{\boldsymbol{k}p}(0)a^\dagger_{\boldsymbol{k}p}(t)\right\rangle_{\mathrm{b_{EM}}} = \mathrm{Tr}_{\mathrm{b_{EM}}}[\hat{a}_{\boldsymbol{k}p}(0)\hat{a}^\dagger_{\boldsymbol{k}p}(t)\hat{\rho}_{\mathrm{b_{EM}}}] = e^{i\omega_{\boldsymbol{k}}t}. \tag{A4}$$

In the limit of a large cavity volume for the EM field $\mathcal{V}_0$, we can replace the sum over cavity modes $\boldsymbol{k}$ with an integral as

$$\frac{1}{\mathcal{V}_0}\sum_{\boldsymbol{k}} \to \frac{1}{(2\pi)^3}\int \mathrm{d}\boldsymbol{k}. \tag{A5}$$

After evaluating the angular part of the integral, we arrive at

$$\begin{aligned}\mathcal{R}^{\mathrm{R}}_{\mathrm{GS,LE}} = \frac{1}{6\hbar\varepsilon_0\pi^2}\sum_{\alpha=x,y,z}\int_0^\infty \mathrm{d}k\int_0^\infty \mathrm{d}t\,c_0k^3 \\ \times\left(\mathcal{L}^{\mathrm{L}}_\alpha e^{\mathcal{L}^{\mathrm{LE,GS}}_{0,\mathrm{s}}t}\mathcal{L}^{\mathrm{R}}_\alpha e^{ic_0kt} + \mathcal{L}^{\mathrm{R}}_\alpha e^{\mathcal{L}^{\mathrm{GS,LE}}_{0,\mathrm{s}}t}\mathcal{L}^{\mathrm{L}}_\alpha e^{-ic_0kt}\right).\end{aligned} \tag{A6}$$

Then, we insert the spectral resolution of $\mathcal{L}_{0,\mathrm{s}}$ acting on the GS-LE coherences ($|\mathrm{GS}\rangle\langle\mathrm{LE}_n|$) and note that all the eigenvalues of this operator are purely imaginary, so we can write these as $\mathcal{L}^{\mathrm{GS,LE}}_{0,\mathrm{s}} = \mathcal{S}^{0,\mathrm{s}}_{\mathrm{GS,LE}}(i\Omega_{\mathrm{GS,LE}})(\mathcal{S}^{0,\mathrm{s}}_{\mathrm{GS,LE}})^{-1}$ and $\mathcal{L}^{\mathrm{LE,GS}}_{0,\mathrm{s}} = \mathcal{S}^{0,\mathrm{s}}_{\mathrm{LE,GS}}(-i\Omega_{\mathrm{LE,GS}})(\mathcal{S}^{0,\mathrm{s}}_{\mathrm{LE,GS}})^{-1}$, where $\Omega_{\mathrm{GS,LE}}$ and $\Omega_{\mathrm{LE,GS}}$ are diagonal matrices with real positive-valued entries. We then evaluate the time integral, noting the imaginary part vanishes, and change variables in the k integral to $\omega = c_0k$ to give

$$\begin{aligned}\mathcal{R}^{\mathrm{R}}_{\mathrm{GS,LE}} = \frac{1}{6\hbar\varepsilon_0c_0^3\pi}\sum_{\alpha=x,y,z}\int_0^\infty \mathrm{d}\omega\,\omega^3 \\ \times\left(\mathcal{L}^{\mathrm{L}}_\alpha\mathcal{S}^{0,\mathrm{s}}_{\mathrm{LE,GS}}\delta(\Omega_{\mathrm{LE,GS}}-\omega)(\mathcal{S}^{0,\mathrm{s}}_{\mathrm{LE,GS}})^{-1}\mathcal{L}^{\mathrm{R}}_\alpha\right. \\ \left. + \mathcal{L}^{\mathrm{R}}_\alpha\mathcal{S}^{0,\mathrm{s}}_{\mathrm{GS,LE}}\delta(\Omega_{\mathrm{GS,LE}}-\omega)(\mathcal{S}^{0,\mathrm{s}}_{\mathrm{GS,LE}})^{-1}\mathcal{L}^{\mathrm{L}}_\alpha\right).\end{aligned} \tag{A7}$$

Integrating over ω then yields the expressions given in Eq. (61). These steps can be repeated for $\mathcal{R}^{\mathrm{R}}_{\mathrm{LE,LE}}$ to obtain Eq. (62), where additionally we discard imaginary terms (which correspond to Lamb shifts).

APPENDIX B: SIMPLIFICATION OF THE DIMER MODEL BATHS

In this appendix, we describe how the three-bath model for the dimer–CT model can be reduced to a two-bath model to speed up exact HEOM calculations. Suppose we have a system coupled to a set of baths, $j = 1,\ldots,N$, with identical frequency distributions but different reorganization energies, i.e., $\mathcal{J}_j(\omega) = \eta_j\,\mathcal{J}_0(\omega)$ with $\eta_j = \lambda_j/\lambda_0$ as in the dimer–CT model considered here. We can write the coupling term for bath modes with frequency $\omega_{j\alpha} = \omega_{0\alpha}$ as

$$\hat{H}_{\mathrm{sb},\alpha} = c_\alpha\,\hat{\boldsymbol{q}}_\alpha\cdot\boldsymbol{\eta}^{1/2}\hat{\boldsymbol{V}}, \tag{B1}$$

where $c_\alpha = c_{0\alpha}$, $[\hat{\boldsymbol{q}}_\alpha]_j = \hat{q}_{j\alpha}$, $[\hat{\boldsymbol{V}}]_j = \hat{V}_j$, and $\boldsymbol{\eta}$ is a diagonal matrix of the values of η_j. We can insert an orthogonal matrix $\mathbf{S}$, to rewrite this as

$$\hat{H}_{\mathrm{sb},\alpha} = c_\alpha\hat{\boldsymbol{q}}^{\mathsf{T}}_\alpha\mathbf{S}^{\mathsf{T}}\mathbf{S}\boldsymbol{\eta}^{1/2}\hat{\boldsymbol{V}} = c_\alpha\hat{\tilde{\boldsymbol{q}}}\cdot\hat{\tilde{\boldsymbol{V}}}. \tag{B2}$$

We can then rewrite the Hamiltonian in terms of a new set of uncorrelated baths with mode displacements $\hat{\tilde{q}}_{j\alpha}$, and coupling operators $\hat{\tilde{V}}_j$. If we choose $\mathbf{S}$ such that one of the new system–bath coupling operators is just proportional to the identity operator $\hat{\tilde{V}}_1 \propto \hat{1}$, then we eliminate coupling between one of the baths and the system and therefore reduce the complexity of the problem. For $\kappa = 1$, we can find such a transformation as follows. First, we write $\boldsymbol{\eta}^{1/2}\hat{\boldsymbol{V}}$ as

$$\boldsymbol{\eta}^{1/2}\hat{\boldsymbol{V}} = \begin{pmatrix}|\mathrm{LE}_1\rangle\langle\mathrm{LE}_1| \\ |\mathrm{LE}_2\rangle\langle\mathrm{LE}_2| + \kappa|\mathrm{CT}\rangle\langle\mathrm{CT}| \\ \sqrt{\eta}|\mathrm{CT}\rangle\langle\mathrm{CT}|\end{pmatrix}, \tag{B3}$$

where $\lambda_0 = \lambda_{\mathrm{LE}}$ and $\eta = \sqrt{\lambda_{\mathrm{CT}}/\lambda_{\mathrm{LE}}}$. We then set $\mathbf{S}$ as

$$\mathbf{S} = \begin{pmatrix} \frac{1}{\sqrt{2}} & \frac{1}{\sqrt{2}} & 0 \\ \frac{1}{\sqrt{2}} & -\frac{1}{\sqrt{2}} & 0 \\ 0 & 0 & 1 \end{pmatrix}, \tag{B4}$$

which gives $\hat{\tilde{\boldsymbol{V}}}$ as

$$\hat{\tilde{\boldsymbol{V}}} = \begin{pmatrix} \frac{1}{\sqrt{2}}\hat{1} \\ \frac{1}{\sqrt{2}}(|\mathrm{LE}_1\rangle\langle\mathrm{LE}_1| - |\mathrm{LE}_2\rangle\langle\mathrm{LE}_2| - |\mathrm{CT}\rangle\langle\mathrm{CT}|) \\ \sqrt{\eta}|\mathrm{CT}\rangle\langle\mathrm{CT}| \end{pmatrix}. \tag{B5}$$

We see that the system coupling operator for the new bath 1 is proportional to an identity operator, so coupling to this bath does not affect the system dynamics and it can eliminated.

For the $\kappa = 0$ case, we set

$$\mathbf{S} = \begin{pmatrix} \frac{1}{\sqrt{2+\eta^{-1}}} & \frac{1}{\sqrt{2+\eta^{-1}}} & \frac{1}{\sqrt{\eta(2+\eta^{-1})}} \\ \frac{1}{\sqrt{2}} & -\frac{1}{\sqrt{2}} & 0 \\ -\frac{1}{\sqrt{2+4\eta}} & -\frac{1}{\sqrt{2+4\eta}} & \frac{2\sqrt{\eta}}{\sqrt{2+4\eta}} \end{pmatrix}, \tag{B6}$$

which gives $\hat{\tilde{\boldsymbol{V}}}$ as

$$\hat{\tilde{\boldsymbol{V}}} = \begin{pmatrix} \frac{1}{\sqrt{2+\eta^{-1}}}\hat{1} \\ \frac{1}{\sqrt{2}}(|\mathrm{LE}_1\rangle\langle\mathrm{LE}_1| - |\mathrm{LE}_2\rangle\langle\mathrm{LE}_2|) \\ \frac{1}{\sqrt{2+4\eta}}(2\eta|\mathrm{CT}\rangle\langle\mathrm{CT}| - |\mathrm{LE}_1\rangle\langle\mathrm{LE}_1| - |\mathrm{LE}_2\rangle\langle\mathrm{LE}_2|) \end{pmatrix}. \tag{B7}$$

Again, bath 1 can be eliminated because its coupling operator is proportional to an identity operator. We note that only the top row of $\mathbf{S}$ is uniquely defined for any κ, by requiring that $\hat{\tilde{V}}_1 \propto \hat{1}$, and the choice for the other rows, and other coupling operators, is not unique.

Finally, we note that we can scale the reorganization energy of a given bath by α if we also scale the corresponding coupling operator by $1/\sqrt{\alpha}$ because the coupling coefficients are proportional to $\sqrt{\lambda_j}$, $c_{j\alpha} \propto \sqrt{\lambda_j}$ without changing the Hamiltonian. The choice does not affect the exact dynamics, but it does affect how the hierarchy is truncated with our reorganization energy weighted cutoff scheme. For the calculations, we set $\lambda_2 = \lambda_{\mathrm{LE}}$ and $\lambda_3 = \lambda_{\mathrm{CT}}$, which means the coupling operator $\hat{\tilde{V}}_3$ given above scaled down by $1/\sqrt{\eta}$.

APPENDIX C: THE INTERNAL CONVERSION TERM

In this appendix, we present a brief justification of the Lindblad form for the internal conversion term used to model direct non-radiative transitions from the Chl∗ states to the ground state in LHCII. The argument is essentially the same as that used to derive the radiative and ET coupling Hamiltonians. We start by assuming that the internal conversion coupling is described by a Hamiltonian of the form

$$\hat{H}_{\mathrm{LE,GS}} = \sum_{n=1}^{N_{\mathrm{LE}}} \left(\hat{X}_n |\mathrm{GS}\rangle\langle \mathrm{LE}_n| + \hat{X}_n^\dagger |\mathrm{LE}_n\rangle\langle \mathrm{GS}| \right), \tag{C1}$$

where we assume the $\hat{X}_n$ operator acts on degrees of freedom other than the b_{LE} degrees of freedom and we also assume that these operators commute at all times. We also assume that the thermal average of $\hat{X}_n$ is zero. The nonadiabatic coupling between the LE states and the ground state depends primarily on local vibrational modes of the chromophore, so it is reasonable to assume that these operators commute.

We can now evaluate the second order Markovian Nakajima–Zwanzig relaxation operator for internal conversion with the projection operator given in the main text. We will further approximate the reference Liouvillian as $\mathcal{L}_0 + \mathcal{V} \approx -\frac{i}{\hbar}[\hat{\Pi}_{\mathrm{LE}} \tilde{E}_{\mathrm{LE}}, \cdot\,] \otimes \mathcal{I}_{\mathrm{ado}}$, where $\tilde{E}_{\mathrm{LE}}$ is the average LE state energy, an approximation that is justified because the mean energy difference between the LE states and the ground state is much larger than the energy differences within the LE manifold. From this, it is straightforward to obtain the relaxation superoperator as

$$\begin{aligned} \mathcal{R}^{\mathrm{NR}}_{\mathrm{LE,LE}}\hat{\sigma} = \sum_{n=1}^{N_{\mathrm{LE}}} \int_0^\infty \mathrm{d}t \Big(& \left\langle X_n^\dagger(t) X_n(0) \right\rangle_{\mathrm{b}'} e^{i\tilde{E}_{\mathrm{LE}}t/\hbar} |\mathrm{LE}_n\rangle\langle \mathrm{LE}_n|\hat{\sigma} \\ & + \left\langle X_n^\dagger(t) X_n(0) \right\rangle_{\mathrm{b}'}^* e^{-i\tilde{E}_{\mathrm{LE}}t/\hbar} \hat{\sigma}|\mathrm{LE}_n\rangle\langle \mathrm{LE}_n| \Big). \end{aligned} \tag{C2}$$

Ignoring Lamb shift terms that originate from the imaginary parts of the $\left\langle X_n^\dagger(t) X_n(0) \right\rangle_{\mathrm{b}'}$ correlation functions, this reduces to

$$\mathcal{R}^{\mathrm{NR}}_{\mathrm{LE,LE}}\hat{\sigma} = -\sum_{n=1}^{N_{\mathrm{LE}}} \frac{k_{\mathrm{NR},n}}{2} \{ |\mathrm{LE}_n\rangle\langle \mathrm{LE}_n|, \hat{\sigma} \}, \tag{C3}$$

where $k_{\mathrm{NR},n}$ is the non-radiative decay rate for internal conversion of state LE_n. The corresponding term in the equation of motion for $\hat{\sigma}_{\mathrm{GS},\mathbf{n}}(t)$ is

$$\mathcal{R}^{\mathrm{NR}}_{\mathrm{GS,LE}}\hat{\sigma} = \sum_{n=1}^{N_{\mathrm{LE}}} k_{\mathrm{NR},n} |\mathrm{GS}\rangle\langle \mathrm{LE}_n|\hat{\sigma}|\mathrm{LE}_n\rangle\langle \mathrm{GS}|. \tag{C4}$$

The reverse internal conversion rate is related to the forward rate by $k^{\mathrm{back}}_{\mathrm{NR},n} = e^{-\beta\tilde{E}_{\mathrm{LE}}} k_{\mathrm{NR},n}$; however, because $\beta\tilde{E}_{\mathrm{LE}}$ is typically very large, we can safely ignore the back reaction terms.

APPENDIX D: ADDITIONAL DETAILS OF THE LHCII MODELS

In this appendix, we list the model parameters used in our simulations of the LHCII monomer. First, the LE system Hamiltonians for the two LHCII models are

$$\mathbf{H}_{\mathrm{LE,s}} = (E_{\mathrm{LE}} + \lambda_{\mathrm{Chl}^*})\mathbf{1} + \begin{pmatrix} 635 & 36 & -5 & -3 & 1 & -2 & -3 & 3 & 4 & -5 & 20 & 2 & -8 & 2 \\ 36 & 70 & 15 & 6 & 0 & 5 & 6 & -6 & -24 & -5 & 1 & 8 & -2 & 0 \\ -5 & 15 & 80 & -1 & 0 & -4 & 6 & 4 & 72 & 7 & -1 & 1 & 1 & -5 \\ -3 & 6 & -1 & 140 & 4 & 71 & 24 & -4 & -2 & 0 & -3 & 3 & 2 & -3 \\ 1 & 0 & 0 & 4 & 775 & 9 & -4 & -4 & 0 & 1 & 1 & -2 & -1 & 0 \\ -2 & 5 & -4 & 71 & 9 & 615 & 16 & -5 & 2 & 0 & -2 & 2 & 2 & -2 \\ -3 & 6 & 6 & 24 & -4 & 16 & 525 & -4 & -5 & 1 & -2 & 3 & 3 & -3 \\ 3 & -6 & 4 & -4 & -4 & -5 & -4 & 395 & 24 & 43 & 5 & -1 & -2 & 1 \\ 4 & -24 & 72 & -2 & 0 & 2 & -5 & 24 & 855 & -2 & 4 & -1 & -2 & 2 \\ -5 & -5 & 7 & 0 & 1 & 0 & 1 & 43 & -2 & 0 & -26 & 13 & 6 & -1 \\ 20 & 1 & -1 & -3 & 1 & -2 & -2 & 5 & 4 & -26 & 150 & 99 & -3 & 1 \\ 2 & 8 & 1 & 3 & -2 & 2 & 3 & -1 & -1 & 13 & 99 & 180 & 0 & 0 \\ -8 & -2 & 1 & 2 & -1 & 2 & 3 & -2 & -2 & 6 & -3 & 0 & 90 & -36 \\ 2 & 0 & -5 & -3 & 0 & -2 & -3 & 1 & 2 & -1 & 1 & 0 & -36 & 200 \end{pmatrix} \mathrm{cm}^{-1} \quad \text{(D1)}$$

for Model 1 and

$$\mathbf{H}_{\mathrm{LE,s}} = (E_{\mathrm{LE}} + \lambda_{\mathrm{D,Chl}^*})\mathbf{1} + \begin{pmatrix} 816.00 & 49.64 & -5.89 & -2.51 & 0.77 & -1.87 & -2.49 & 2.78 & 3.79 & -5.95 & 24.89 & 9.13 & -10.79 & 3.59 \\ 49.64 & 84.00 & 38.11 & 6.42 & -0.71 & 5.60 & 7.13 & -5.84 & -19.25 & -11.39 & 9.69 & 15.83 & -4.96 & 0.69 \\ -5.89 & 38.11 & 214.00 & -3.28 & 1.13 & -8.89 & 1.23 & 6.72 & 96.66 & 12.97 & -2.70 & -0.76 & 2.68 & -6.70 \\ -2.51 & 6.42 & -3.28 & 387.00 & 3.35 & 104.56 & 35.93 & -2.76 & -7.28 & -4.18 & -3.80 & 4.67 & 2.12 & -3.42 \\ 0.77 & -0.71 & 1.13 & 3.35 & 606.00 & 29.71 & -4.47 & -5.13 & -0.77 & 1.61 & 1.33 & -2.85 & -1.40 & 0.37 \\ -1.87 & 5.60 & -8.89 & 104.56 & 29.71 & 777.00 & 59.38 & -4.99 & -0.16 & -3.28 & -2.52 & 3.10 & 1.47 & -2.16 \\ -2.49 & 7.13 & 1.23 & 35.93 & -4.47 & 59.38 & 641.00 & -4.43 & -11.99 & -0.14 & -2.78 & 3.07 & 2.20 & -3.25 \\ 2.78 & -5.84 & 6.72 & -2.76 & -5.13 & -4.99 & -4.43 & 688.00 & 36.07 & 61.97 & 4.35 & -1.08 & -2.01 & 1.30 \\ 3.79 & -19.25 & 96.66 & -7.28 & -0.77 & -0.16 & -11.99 & 36.07 & 648.00 & 3.86 & 4.30 & -2.57 & -2.92 & 2.33 \\ -5.95 & -11.39 & 12.97 & -4.18 & 1.61 & -3.28 & -0.14 & 61.97 & 3.86 & 0.00 & -24.96 & 23.10 & 7.21 & -1.55 \\ 24.89 & 9.69 & -2.70 & -3.80 & 1.33 & -2.52 & -2.78 & 4.35 & 4.30 & -24.96 & 39.00 & 126.92 & -6.15 & 4.55 \\ 9.13 & 15.83 & -0.76 & 4.67 & -2.85 & 3.10 & 3.07 & -1.08 & -2.57 & 23.10 & 126.92 & 21.00 & -0.47 & -0.18 \\ -10.79 & -4.96 & 2.68 & 2.12 & -1.40 & 1.47 & 2.20 & -2.01 & -2.92 & 7.21 & -6.15 & -0.47 & 101.00 & -50.22 \\ 3.59 & 0.69 & -6.70 & -3.42 & 0.37 & -2.16 & -3.25 & 1.30 & 2.33 & -1.55 & 4.55 & -0.18 & -50.22 & 187.00 \end{pmatrix} \mathrm{cm}^{-1} \quad \text{(D2)}$$

for Model 2. The columns/rows correspond to the states in the following order: $b601^*$, $a602^*$, $a603^*$, $a604^*$, $b605^*$, $b606^*$, $b607^*$, $b608^*$, $b609^*$, $a610^*$, $a611^*$, $a612^*$, $a613^*$, and $a614^*$. We incorporate the reorganization energy contribution of the LE baths into the system Hamiltonian matrices, $\mathbf{H}_{\mathrm{LE,s}}$, and as such diagonal elements correspond to vertical excitation energies in the absence of LE coupling, and the diagonal element minus $\lambda_{\mathrm{D,Chl}^*}$ is the free energy of that LE state in the absence of inter-LE state coupling. The CT state system Hamiltonians are given by

$$\hat{H}_{\mathrm{CT_1,s}} = (E_{a612^*} + \Delta G_{\mathrm{CT1}})|\mathrm{CT_1}\rangle\langle\mathrm{CT_1}|, \quad \text{(D3)}$$

$$\hat{H}_{\mathrm{CT_2,s}} = (E_{a603^*} + \Delta G_{\mathrm{CT2}})|\mathrm{CT_2}\rangle\langle\mathrm{CT_2}|, \quad \text{(D4)}$$

where E_{a612^*} and E_{a603^*} are the diagonal elements of $\mathbf{H}_{\mathrm{LE,s}}$ corresponding the states $a612^*$ and $a603^*$, respectively. Here, $\mathrm{CT_1}$ is the $a612^-\mathrm{Lut1}^+$ state and $\mathrm{CT_2}$ is the $a603^-\mathrm{Lut2}^+$ state. Finally, $\hat{H}_{\mathrm{GS,s}} = 0$ by definition. The remaining model parameters are listed in Table I.

TABLE I. Parameters used for the LHCII monomer CT quenching models.

Parameter	Value (cm^{-1} unless specified otherwise)
ΔG_{CT1}	−82
λ_{CT1}	5 405
V_{CT1}	240
ΔG_{CT2}	951
λ_{CT2}	5 052
V_{CT2}	279
$\omega_{D,CT}$	30
Ω	1 500
γ	50
E_{LE} (Model 1)	14 780
E_{LE} (Model 2)	15 073
λ_{D,Chl^*}	220
ω_{D,Chl^*}	353.6777
μ_{Chla} (D)	4.0
μ_{Chlb} (D)	3.4
k_{NR} (ns^{-1})	0.25

The $G^B_{AB}(t)$ and $G^B_{BA}(t)$ functions were evaluated using[56,58]

$$G^B_{AB}(t) = G^B_{BA}(t)^* = \exp(\zeta_{AB}(t) + i\Delta\epsilon_{AB}t/\hbar), \tag{D5}$$

$$\zeta_{AB}(t) = -\int_0^\infty d\omega \frac{\mathcal{J}_{AB}(\omega)}{\omega^2} \times \left[\coth\left(\frac{\beta\hbar\omega}{2}\right)(1-\cos(\omega t)) + i\,\sin(\omega t)\right], \tag{D6}$$

where $\mathcal{J}_{AB}(\omega)$ is the b_{CT} spectral density associated with the $A \to B$ charge transfer and $\Delta\epsilon_{AB}$ is the free energy change excluding b_{LE} contributions (i.e., the free energy change with $\hat{B}_{n,r} = 0$). In order to evaluate the integrals over these functions, each component of the spectral density (the Debye and Brownian Oscillator components) was discretized into 512 frequencies using a Gauss–Legendre quadrature for the function $(1/(4\pi\lambda))\mathcal{J}_{D/BO}(\omega)/\omega$,[94] and using this, the $\zeta_{AB}(t)$ function was evaluated and the required numerical integrals were evaluated using the trapezium rule. The integrals were evaluated up to t_{max} = 23.5 fs, discretized into 1000 time points for the CT-LE correlation functions and 14 104 time points for the much more oscillatory CT-GS correlation functions. The same expressions and methodology were used to evaluate the ET kernel for the dimer model in Sec. IV.

REFERENCES

[1] T. Mirkovic, E. E. Ostroumov, J. M. Anna, R. van Grondelle, G. Govindjee, and G. D. Scholes, "Light absorption and energy transfer in the antenna complexes of photosynthetic organisms," Chem. Rev. **117**, 249–293 (2017).

[2] D. J. Vinyard, G. M. Ananyev, and G. Charles Dismukes, "Photosystem II: The reaction center of oxygenic photosynthesis," Annu. Rev. Biochem. **82**, 577–606 (2013).

[3] M. Gorka, A. Baldansuren, A. Malnati, E. Gruszecki, J. H. Golbeck, and K. V. Lakshmi, "Shedding light on primary donors in photosynthetic reaction centers," Front. Microbiol. **12**, 735666 (2021).

[4] *Molecular Mechanisms of Photosynthesis*, edited by R. E. Blankenship (Blackwell Science Ltd., Oxford, UK, 2002).

[5] R. Croce and H. van Amerongen, "Light-harvesting and structural organization of photosystem II: From individual complexes to thylakoid membrane," J. Photochem. Photobiol., B **104**, 142–153 (2011).

[6] R. Goss and B. Lepetit, "Biodiversity of NPQ," J. Plant Physiol. **172**, 13–32 (2015).

[7] S. Park, C. J. Steen, D. Lyska, A. L. Fischer, B. Endelman, M. Iwai, K. K. Niyogi, and G. R. Fleming, "Chlorophyll–carotenoid excitation energy transfer and charge transfer in *Nannochloropsis oceanica* for the regulation of photosynthesis," Proc. Natl. Acad. Sci. U. S. A. **116**, 3385–3390 (2019).

[8] A. V. Ruban and F. Saccon, "Chlorophyll *a* de-excitation pathways in the LHCII antenna," J. Chem. Phys. **156**, 070902 (2022).

[9] A. Pinnola, H. Staleva-Musto, S. Capaldi, M. Ballottari, R. Bassi, and T. Polívka, "Electron transfer between carotenoid and chlorophyll contributes to quenching in the LHCSR1 protein from *Physcomitrella patens*," Biochim. Biophys. Acta, Bioenerg. **1857**, 1870–1878 (2016).

[10] E. E. Ostroumov, J. P. Götze, M. Reus, P. H. Lambrev, and A. R. Holzwarth, "Characterization of fluorescent chlorophyll charge-transfer states as intermediates in the excited state quenching of light-harvesting complex II," Photosynth. Res. **144**, 171–193 (2020).

[11] Y. Tanimura and R. Kubo, "Time evolution of a quantum system in contact with a nearly Gaussian-Markoffian noise bath," J. Phys. Soc. Jpn. **58**, 101–114 (1989).

[12] A. Ishizaki and G. R. Fleming, "Theoretical examination of quantum coherence in a photosynthetic system at physiological temperature," Proc. Natl. Acad. Sci. U. S. A. **106**, 17255–17260 (2009).

[13] Y. Tanimura, "Numerically 'exact' approach to open quantum dynamics: The hierarchical equations of motion (HEOM)," J. Chem. Phys. **153**, 020901 (2020).

[14] A. Ishizaki and G. R. Fleming, "Unified treatment of quantum coherent and incoherent hopping dynamics in electronic energy transfer: Reduced hierarchy equation approach," J. Chem. Phys. **130**, 234111 (2009).

[15] M. Sarovar, A. Ishizaki, G. R. Fleming, and K. B. Whaley, "Quantum entanglement in photosynthetic light-harvesting complexes," Nat. Phys. **6**, 462–467 (2010); arXiv:0905.3787.

[16] J. Strümpfer and K. Schulten, "Light harvesting complex II B850 excitation dynamics," J. Chem. Phys. **131**, 225101 (2009).

[17] A. Ishizaki, T. R. Calhoun, G. S. Schlau-Cohen, and G. R. Fleming, "Quantum coherence and its interplay with protein environments in photosynthetic electronic energy transfer," Phys. Chem. Chem. Phys. **12**, 7319 (2010).

[18] L. Chen, R. Zheng, Y. Jing, and Q. Shi, "Simulation of the two-dimensional electronic spectra of the Fenna-Matthews-Olson complex using the hierarchical equations of motion method," J. Chem. Phys. **134**, 194508 (2011).

[19] C. Kreisbeck, T. Kramer, M. Rodríguez, and B. Hein, "High-performance solution of hierarchical equations of motion for studying energy transfer in light-harvesting complexes," J. Chem. Theory Comput. **7**, 2166–2174 (2011).

[20] A. G. Dijkstra and Y. Tanimura, "The role of the environment time scale in light-harvesting efficiency and coherent oscillations," New J. Phys. **14**, 073027 (2012).

[21] C. Kreisbeck, T. Kramer, and A. Aspuru-Guzik, "Scalable high-performance algorithm for the simulation of exciton dynamics. Application to the light-harvesting complex II in the presence of resonant vibrational modes," J. Chem. Theory Comput. **10**, 4045–4054 (2014).

[22] M. Schröter, T. Pullerits, and O. Kühn, "Unraveling the quantum state mixing of excitonic and vibronic excitations in the dynamics of molecular aggregates," Ann. Phys. **527**, 536–545 (2015).

[23] H. C. H. Chan, O. E. Gamel, G. R. Fleming, and K. B. Whaley, "Single-photon absorption by single photosynthetic light-harvesting complexes," J. Phys. B: At., Mol. Opt. Phys. **51**, 054002 (2018); arXiv:1801.04924.

[24] V. Janković and T. Mančal, "Exact description of excitonic dynamics in molecular aggregates weakly driven by light," J. Chem. Phys. **153**, 244122 (2020); arXiv:2001.07180.

[25] Y. Yan, Y. Liu, T. Xing, and Q. Shi, "Theoretical study of excitation energy transfer and nonlinear spectroscopy of photosynthetic light-harvesting complexes using the nonperturbative reduced dynamics method," Wiley Interdiscip. Rev.: Comput. Mol. Sci. **11**, e1498 (2021).

[26] V. I. Novoderezhkin, R. Croce, M. Wahadoszamen, I. Polukhina, E. Romero, and R. van Grondelle, "Mixing of exciton and charge-transfer states in light-harvesting complex Lhca4," Phys. Chem. Chem. Phys. **18**, 19368–19377 (2016).

[27]J. Blumberger, "Recent advances in the theory and molecular simulation of biological electron transfer reactions," Chem. Rev. **115**, 11191–11238 (2015).
[28]Q. Shi, L. Chen, G. Nan, R.-X. Xu, and Y. Yan, "Efficient hierarchical Liouville space propagator to quantum dissipative dynamics," J. Chem. Phys. **130**, 084105 (2009).
[29]Q. Shi, L. Chen, G. Nan, R. Xu, and Y. Yan, "Electron transfer dynamics: Zusman equation versus exact theory," J. Chem. Phys. **130**, 164518 (2009).
[30]T. Firmino, E. Mangaud, F. Cailliez, A. Devolder, D. Mendive-Tapia, F. Gatti, C. Meier, M. Desouter-Lecomte, and A. de la Lande, "Quantum effects in ultrafast electron transfers within cryptochromes," Phys. Chem. Chem. Phys. **18**, 21442–21457 (2016).
[31]Q. Shi, Y. Xu, Y. Yan, and M. Xu, "Efficient propagation of the hierarchical equations of motion using the matrix product state method," J. Chem. Phys. **148**, 174102 (2018).
[32]R. Borrelli, "Density matrix dynamics in twin-formulation: An efficient methodology based on tensor-train representation of reduced equations of motion," J. Chem. Phys. **150**, 234102 (2019).
[33]Y. Ke, R. Borrelli, and M. Thoss, "Hierarchical equations of motion approach to hybrid fermionic and bosonic environments: Matrix product state formulation in twin space," J. Chem. Phys. **156**, 194102 (2022); arXiv:2202.10273.
[34]Y. Yan, M. Xu, T. Li, and Q. Shi, "Efficient propagation of the hierarchical equations of motion using the Tucker and hierarchical Tucker tensors," J. Chem. Phys. **154**, 194104 (2021).
[35]L. P. Lindoy, Ph.D. thesis, University of Oxford, 2019.
[36]M. Richter and B. P. Fingerhut, "Electron transfer pathways and dynamics in *Drosophila* cryptochrome - the role of protein electrostatics," EPJ Web Conf. **205**, 10009 (2019).
[37]M. Richter and B. P. Fingerhut, "Coupled excitation energy and charge transfer dynamics in reaction centre inspired model systems," Faraday Discuss. **216**, 72–93 (2019).
[38]N. Makri and D. E. Makarov, "Tensor propagator for iterative quantum time evolution of reduced density matrices. I. Theory," J. Chem. Phys. **102**, 4600–4610 (1995).
[39]N. Makri, "Quantum dissipative dynamics: A numerically exact methodology," J. Phys. Chem. A **102**, 4414–4427 (1998).
[40]N. Makri, "Small matrix disentanglement of the path integral: Overcoming the exponential tensor scaling with memory length," J. Chem. Phys. **152**, 041104 (2020).
[41]S. Kundu and N. Makri, "Real-time path integral simulation of exciton-vibration dynamics in light-harvesting bacteriochlorophyll aggregates," J. Phys. Chem. Lett. **11**, 8783–8789 (2020).
[42]S. Kundu, R. Dani, and N. Makri, "B800-to-B850 relaxation of excitation energy in bacterial light harvesting: All-state, all-mode path integral simulations," J. Chem. Phys. **157**, 015101 (2022).
[43]W. M. Zhang, T. Meier, V. Chernyak, and S. Mukamel, "Exciton-migration and three-pulse femtosecond optical spectroscopies of photosynthetic antenna complexes," J. Chem. Phys. **108**, 7763–7774 (1998).
[44]G. D. Scholes and G. R. Fleming, "On the mechanism of light harvesting in photosynthetic purple bacteria: B800 to B850 energy transfer," J. Phys. Chem. B **104**, 1854–1868 (2000).
[45]V. I. Novoderezhkin and R. van Grondelle, "Physical origins and models of energy transfer in photosynthetic light-harvesting," Phys. Chem. Chem. Phys. **12**, 7352 (2010).
[46]V. Novoderezhkin, A. Marin, and R. van Grondelle, "Intra- and inter-monomeric transfers in the light harvesting LHCII complex: The Redfield–Förster picture," Phys. Chem. Chem. Phys. **13**, 17093 (2011).
[47]V. I. Novoderezhkin, R. Croce, and R. van Grondelle, "Dynamics of the mixed exciton and charge-transfer states in light-harvesting complex Lhca4: Hierarchical equation approach," Biochim. Biophys. Acta, Bioenerg. **1859**, 655–665 (2018).
[48]A. Kelly and Y. M. Rhee, "Mixed quantum-classical description of excitation energy transfer in a model Fenna-Matthews-Olsen complex," J. Phys. Chem. Lett. **2**, 808–812 (2011).
[49]P. Huo and D. F. Coker, "Communication: Partial linearized density matrix dynamics for dissipative, non-adiabatic quantum evolution," J. Chem. Phys. **135**, 201101 (2011).
[50]H. W. Kim, A. Kelly, J. W. Park, and Y. M. Rhee, "All-atom semiclassical dynamics study of quantum coherence in photosynthetic Fenna–Matthews–Olson complex," J. Am. Chem. Soc. **134**, 11640–11651 (2012).
[51]W. C. Pfalzgraff, A. Montoya-Castillo, A. Kelly, and T. E. Markland, "Efficient construction of generalized master equation memory kernels for multi-state systems from nonadiabatic quantum-classical dynamics," J. Chem. Phys. **150**, 244109 (2019); arXiv:1903.09608.
[52]J. E. Runeson and J. O. Richardson, "Generalized spin mapping for quantum-classical dynamics," J. Chem. Phys. **152**, 084110 (2020); arXiv:1912.10906.
[53]J. R. Mannouch and J. O. Richardson, "A partially linearized spin-mapping approach for nonadiabatic dynamics. I. Derivation of the theory," J. Chem. Phys. **153**, 194109 (2020); arXiv:2007.05047.
[54]J. E. Runeson, J. E. Lawrence, J. R. Mannouch, and J. O. Richardson, "Explaining the efficiency of photosynthesis: Quantum uncertainty or classical vibrations?," J. Phys. Chem. Lett. **13**, 3392–3399 (2022).
[55]M. Sparpaglione and S. Mukamel, "Dielectric friction and the transition from adiabatic to nonadiabatic electron transfer. I. Solvation dynamics in Liouville space," J. Chem. Phys. **88**, 3263–3280 (1988).
[56]T. P. Fay, L. P. Lindoy, and D. E. Manolopoulos, "Spin-selective electron transfer reactions of radical pairs: Beyond the Haberkorn master equation," J. Chem. Phys. **149**, 064107 (2018); arXiv:1808.03211.
[57]T. P. Fay, "Chirality-induced spin coherence in electron transfer reactions," J. Phys. Chem. Lett. **12**, 1407–1412 (2021); arXiv:2101.03104.
[58]T. P. Fay and D. T. Limmer, "Origin of chirality induced spin selectivity in photoinduced electron transfer," Nano Lett. **21**, 6696–6702 (2021); arXiv:2106.06554.
[59]M. Thoss, H. Wang, and W. H. Miller, "Self-consistent hybrid approach for complex systems: Application to the spin-boson model with Debye spectral density," J. Chem. Phys. **115**, 2991–3005 (2001).
[60]T. C. Berkelbach, D. R. Reichman, and T. E. Markland, "Reduced density matrix hybrid approach: An efficient and accurate method for adiabatic and non-adiabatic quantum dynamics," J. Chem. Phys. **136**, 034113 (2012).
[61]A. Montoya-Castillo, T. C. Berkelbach, and D. R. Reichman, "Extending the applicability of Redfield theories into highly non-Markovian regimes," J. Chem. Phys. **143**, 194108 (2015).
[62]A. J. Schile and D. T. Limmer, "Simulating conical intersection dynamics in the condensed phase with hybrid quantum master equations," J. Chem. Phys. **151**, 014106 (2019).
[63]S. Nakajima, "On quantum theory of transport phenomena," Prog. Theor. Phys. **20**, 948–959 (1958).
[64]R. Zwanzig, "Ensemble method in the theory of irreversibility," J. Chem. Phys. **33**, 1338–1341 (1960).
[65]H. Mori, "Transport, collective motion, and Brownian motion," Prog. Theor. Phys. **33**, 423–455 (1965).
[66]F. Müh, M. E.-A. Madjet, and T. Renger, "Structure-based identification of energy sinks in plant light-harvesting complex II," J. Phys. Chem. B **114**, 13517–13535 (2010).
[67]L. Cupellini, D. Calvani, D. Jacquemin, and B. Mennucci, "Charge transfer from the carotenoid can quench chlorophyll excitation in antenna complexes of plants," Nat. Commun. **11**, 662 (2020).
[68]Z. Liu, H. Yan, K. Wang, T. Kuang, J. Zhang, L. Gui, X. An, and W. Chang, "Crystal structure of spinach major light-harvesting complex at 2.72 Å resolution," Nature **428**, 287–292 (2004).
[69]R. Bennett, T. M. Barlow, and A. Beige, "A physically motivated quantization of the electromagnetic field," Eur. J. Phys. **37**, 014001 (2016); arXiv:1506.03305.
[70]M. K. Lee and D. F. Coker, "Modeling electronic-nuclear interactions for excitation energy transfer processes in light-harvesting complexes," J. Phys. Chem. Lett. **7**, 3171–3178 (2016).
[71]J. Segarra-Martí, F. Segatta, T. A. Mackenzie, A. Nenov, I. Rivalta, M. J. Bearpark, and M. Garavelli, "Modeling multidimensional spectral lineshapes from first principles: Application to water-solvated adenine," Faraday Discuss. **221**, 219–244 (2020).
[72]T. J. Zuehlsdorff, S. V. Shedge, S.-Y. Lu, H. Hong, V. P. Aguirre, L. Shi, and C. M. Isborn, "Vibronic and environmental effects in simulations of optical spectroscopy," Annu. Rev. Phys. Chem. **72**, 165–188 (2021).

[73]A. Ishizaki and Y. Tanimura, "Quantum dynamics of system strongly coupled to low-temperature colored noise bath: Reduced hierarchy equations approach," J. Phys. Soc. Jpn. **74**, 3131–3134 (2005).
[74]T. Ikeda and A. Nakayama, "Collective bath coordinate mapping of 'hierarchy' in hierarchical equations of motion," J. Chem. Phys. **156**, 104104 (2022); arXiv:2112.09861.
[75]L. Ko, R. L. Cook, and K. B. Whaley, "Dynamics of photosynthetic light harvesting systems interacting with N-photon Fock states," J. Chem. Phys. **156**, 244108 (2022); arXiv:2111.06996.
[76]R. A. Marcus, "On the theory of oxidation-reduction reactions involving electron transfer. I," J. Chem. Phys. **24**, 966–978 (1956).
[77]N. S. Hush, "Adiabatic rate processes at electrodes. I. Energy-charge relationships," J. Chem. Phys. **28**, 962–972 (1958).
[78]T. P. Fay, "A simple improved low temperature correction for the hierarchical equations of motion," J. Chem. Phys. **157**, 054108 (2022); arXiv:2205.09270.
[79]A. V. Ruban and S. Wilson, "The mechanism of non-photochemical quenching in plants: Localization and driving forces," Plant Cell Physiol. **62**, 1063–1072 (2021).
[80]D. I. G. Bennett, K. Amarnath, and G. R. Fleming, "A structure-based model of energy transfer reveals the principles of light harvesting in photosystem II supercomplexes," J. Am. Chem. Soc. **135**, 9164–9173 (2013).
[81]S. Bourne Worster, C. Stross, F. M. W. C. Vaughan, N. Linden, and F. R. Manby, "Structure and efficiency in bacterial photosynthetic light-harvesting," J. Phys. Chem. Lett. **10**, 7383–7390 (2019); arXiv:1908.08373.
[82]T. P. Fay, "heom-lab: A Matlab code for performing HEOM calculations," https://github.com/tomfay/heom-lab, 2022.
[83]V. Balevičius, K. F. Fox, W. P. Bricker, S. Jurinovich, I. G. Prandi, B. Mennucci, and C. D. P. Duffy, "Fine control of chlorophyll-carotenoid interactions defines the functionality of light-harvesting proteins in plants," Sci. Rep. **7**, 13956 (2017).
[84]A. H. Short, T. P. Fay, T. Crisanto, J. Hall, C. J. Steen, K. K. Niyogi, D. T. Limmer, and G. R. Fleming, "Xanthophyll-cycle based model of the rapid photoprotection of *Nannochloropsis* in response to regular and irregular light/dark sequences," J. Chem. Phys. **156**, 205102 (2022).
[85]A. Chrysafoudi, S. Maity, U. Kleinekathöfer, and V. Daskalakis, "Robust strategy for photoprotection in the light-harvesting antenna of diatoms: A molecular dynamics study," J. Phys. Chem. Lett. **12**, 9626–9633 (2021).
[86]V. Daskalakis, S. Papadatos, and T. Stergiannakos, "The conformational phase space of the photoprotective switch in the major light harvesting complex II," Chem. Commun. **56**, 11215–11218 (2020).
[87]M. Lapillo, E. Cignoni, L. Cupellini, and B. Mennucci, "The energy transfer model of nonphotochemical quenching: Lessons from the minor CP29 antenna complex of plants," Biochim. Biophys. Acta, Bioenerg. **1861**, 148282 (2020).
[88]S. Maity, V. Daskalakis, M. Elstner, and U. Kleinekathöfer, "Multiscale QM/MM molecular dynamics simulations of the trimeric major light-harvesting complex II," Phys. Chem. Chem. Phys. **23**, 7407–7417 (2021).
[89]J. E. Lawrence and D. E. Manolopoulos, "Path integral methods for reaction rates in complex systems," Faraday Discuss. **221**, 9–29 (2020).
[90]E. Rabani, S. A. Egorov, and B. J. Berne, "Classical approximation to nonradiative electronic relaxation in condensed phase systems," J. Phys. Chem. A **103**, 9539–9544 (1999).
[91]S. A. Egorov, E. Rabani, and B. J. Berne, "On the adequacy of mixed quantum-classical dynamics in condensed phase systems," J. Phys. Chem. B **103**, 10978–10991 (1999).
[92]Z. Tong, X. Gao, M. S. Cheung, B. D. Dunietz, E. Geva, and X. Sun, "Charge transfer rate constants for the carotenoid-porphyrin-C_{60} molecular triad dissolved in tetrahydrofuran: The spin-boson model vs the linearized semiclassical approximation," J. Chem. Phys. **153**, 044105 (2020).
[93]J. E. Lawrence and D. E. Manolopoulos, "Analytic continuation of Wolynes theory into the Marcus inverted regime," J. Chem. Phys. **148**, 102313 (2018); arXiv:1710.11113.
[94]J. E. Lawrence and D. E. Manolopoulos, "An improved path-integral method for golden-rule rates," J. Chem. Phys. **153**, 154113 (2020).
[95]H.-P. Breuer, B. Kappler, and F. Petruccione, "The time-convolutionless projection operator technique in the quantum theory of dissipation and decoherence," Ann. Phys. **291**, 36–70 (2001).
[96]E. Cignoni, V. Slama, L. Cupellini, and B. Mennucci, "The atomistic modeling of light-harvesting complexes from the physical models to the computational protocol," J. Chem. Phys. **156**, 120901 (2022).